NTNU – Trondheim
Norwegian University of
Science and Technology

Hydrogen production from biomass derived compounds by sorption enhanced reforming

Guillermo Martinez Sanchez

Chemical Engineering
Submission date: June 2013
Supervisor: De Chen, IKP

Norwegian University of Science and Technology
Department of Chemical Engineering

ACKNOWLEDGEMENT

Abstract

Sorption enhance steam reforming (SESR) is a technique which involves the integration of three reactions in one stage; namely steam reforming (SR), water gas shift (WGS) and CO_2 sorption

This project was developed to study the Water Gas Shift reaction at high temperature in a packed bed reactor. All reactions were carried out with a Trimetallic (Pd/Co-Ni/HT) catalyst with different Pd loadings and analyzed by gas chromatography.

Rate expressions from different mechanisms were analyzed in order to identify the more proper catalytic water gas pathway over the Trimetallic catalyst.

Furthermore, sorption enhanced water gas shift reaction, using dolomite as sorbent, was studied by means of conversion and sorption strength.

Index

Introduction

Nowadays Hydrogen has many applications into the chemical and petrochemical industry. Also it has been identified as a possible energy carrier, both, as an electron donator for fuel cells in future commercial vehicles, as well as a basis component in liquid fuel conversion.

Although considered the simplest and most abundant element on earth (about 75% out of existing matter contains it), is hardly to find it into its elementary form, usually is bonded with other elements, organic or inorganic, such is the examples of water, biomass and natural gas.

The processing of these substances for acquiring hydrogen in its pure form is a difficult and expensive technique. Presently, Natural gas is used as the main organic source to produce hydrogen via steam reforming, unfortunately it has been predicted that petroleum resources have been declining [1], leading to a partial and continuous cost increment, forcing the society to find alternative sources. The continuous change-over of feedstock from fossil to renewable is emerging as an inevitable necessity.

All biomass oxygenated compounds (CnHmOp) are a plenty and cheap source for hydrogen production. A maximum yield will be the result of highly efficient and suitable processes.

Sorption enhance steam reforming is the combination of the traditional steam reforming (SR) and water gas shift (WGS) reactions for H_2 production, but despite of the old-style processes, this technique involves the addition of CO_2 sorption and the performance of all reactions in a single unit.

The changes among CO/CO_2 ratio, owing to the CO_2 sorption reaction, will shift the equilibrium of the SR and WGS reactions. To stabilize those changes a new equilibrium is established. From previous works it has been observed that the new partial composition of the reaction products has achieved a higher H_2 yield[2-6,13].

In order to enhance a high H_2 yield, a suitable catalyst is required. Based on previous works[2-6,13,14] and the good stability, activity and selectivity for WGS and SR, Palladium, Nickel and Cobalt have been chosen to develop the present study. In addition hydrotalcite (HT)-like materials was selected to be the support of this tri-metallic catalyst.

1. Theory

1.1 Biomass.

The United States annually wasted more tones of biomass-carbon-source as "trash" than the consumed from petroleum resources[20]; this means that biomass can highly reduce the dependence of petroleum.

Among the benefits of biomass against petroleum we can highlight the following points:

- Biomass resources are renewable.
- Biomass resource needs are available
- Refining of these resources will create a large number of jobs, since biomass can be found everywhere
- Reduce the toxic burden associated

Only four basic chemical structures present in biomass are of significance for production of fuels and industrial products:

> **Saccharides and polysaccharides (sugars, starches, cellulose, hemicellulose)**

Their basic chemical structure is CH_2O. Most hydroxycarbons occur naturally as either five- or six-membered ring structures. This ring structure may include only one or two connected rings (sugars) or they may be very long polymer chains (cellulose and hemicellulose). [20]

The basic six-sided saccharide structure is exemplified by glucose Long-chain polymers. Glucose or other hexoses are mainly categorized as starch or cellulose **(figure 1.1).**

> **Lignins (Polyphenols)**

Lignin is a network polymer structured upon multi-substituted, methoxy, arylpropane, and hydroxyphenol units.

> **Triacylglycerides or lipids (vegetable oils and animal fats)**

A three-carbon hydroxycarbon, dehydrated glycerol, with three medium to longchain fatty acids attached.

> **Proteins (vegetable and animal polymers made up of amino acids)**

Proteins are long-chain polyamides based solely upon amino acid units.

The use of biomass in the chemical and petrochemical industry has relied mainly on the usage of polysaccharide, lignocellulosic (biomass composed from cellulose, hemicellulose and lignin), and triacylglyceride feedstock. [20]
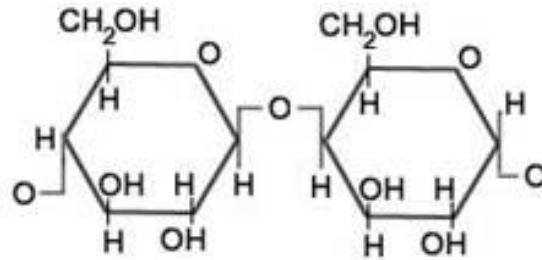
Figure 1.1 six-sided saccharide structure of Cellulose[26]

1.2 Process

As seen in **figure 1.2**, a range of different processes will lead to the development of unique products and co-product. According to the main approach of this study it's important to prioritize the processes involved in the production of Syngas, which are:

- **Pyrolysis**

Treatment of biomass at moderate temperatures (300 to 600ºC) in the absence of O_2 to produce a partial depolymerization of the material.

- **Gasification**

Is a biomass pyrolysis process at a higher temperature (> 700), which is carried out through the addition of water vapor to produce methane and light hydrocarbons, which are reformed to produce synthesis gas (gas synthesis).

- **Thermochemical Liquefaction**

Is a Pyrolytic processing with addition of H_2, CO, CO_2 and selected catalysts (sodium or potassium carbonate and potassium hydroxide[21]) to convert the biomass into hydrocarbons, mixed phenols.
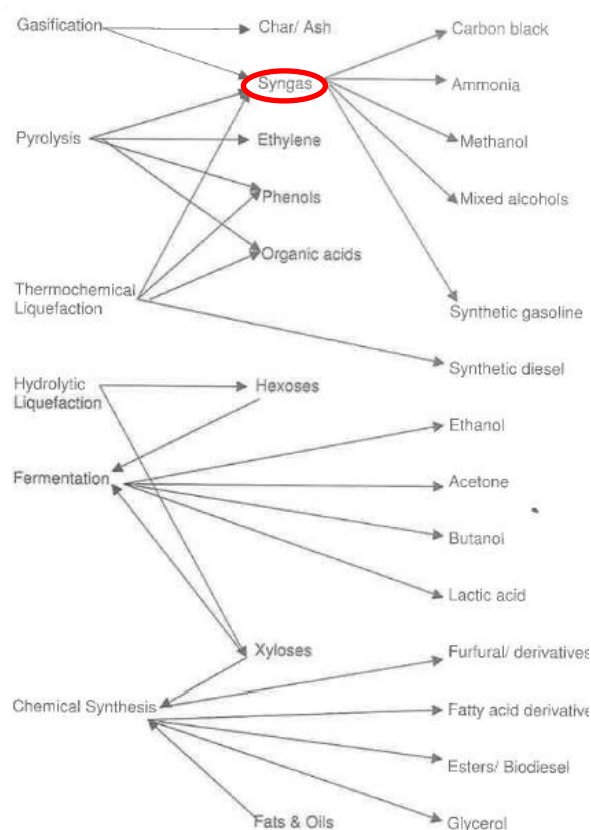
Figure 1.2.- Biomass-derived industrial organic chemicals.

Despite that the processes of pyrolysis and hydrolytic liquefaction generate syngas; H_2 is not catalogued as profitable product, being bio-oil their main yield[22], instead H_2 is recycled. In pyrolysis, is used as combustion gas meanwhile at HL is used either as heating source or process reactant [23].

1.2.1 Hydrogen Production via Gasification Pathway

Biomass has, on average composition of 6 wt % of hydrogen[24,25], which would make it, in principle, a "cheerless" source for H2 production. Nevertheless, H_2 can become a profitable yield by the implementation of the traditional processes after the gasification, namely, Steam reforming and Water Gas Shift. In fact, a raw gasification gas contains 48-55 vol %, dry basis[25], which makes it as feedstock for the process of SR. Schematic diagram a conceptual biomass reforming process is displayed in **figure 1.3**. In addition, for a pure Hydrogen product, after LTS, several "purification" techniques are used, such as PSA (pressure sing absorption), membrane separation, wet scrubbing and cryogenic separation, being PSA highly reliable for a desired purity of 99.9%[27].
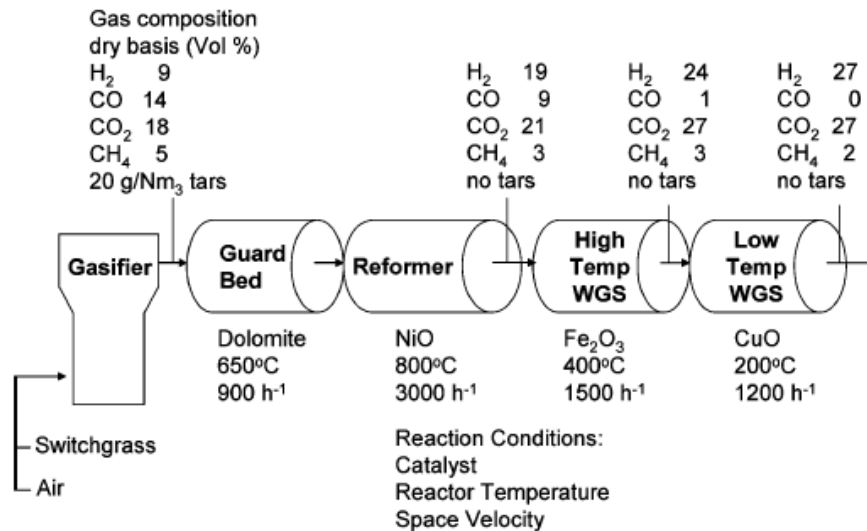
Figure 1.3.- Syngas production from gasification process design. [28]

1.2.1.1 Gasification

Gasification process involves a rapid and continuous denaturalization caused by the temperature increase in biomass. According to the desired performance and products, gasification can be held between 3 different reactor designs (**Figure 1.4**), these are:

Updraft gasifier
Biomass flows from top toward the bottom of the reactor, whilst oxygen/steam enters from the bottom flowing upward. The higher contact time between the hot inlet gases with biomass makes this reactor a suitable and efficient energy recover technology for feeds with high moisture content, even this technology can be used for small-scale applications, unfortunately high tar levels of approximately 100 g/Nm3 are produced [29].Product gas leaves at the top of the reactor

Downdraft gasifier
Biomass and oxygen/steam flows from top toward the bottom of the reactor. Unlike the updraft gasifier this technology yields lower tar level, approximately 1 g/Nm3, unfortunately[29]   feed is restricted upon moisture content, which shouldn't exceed 20%. Product gas leaves at the bottom of the reactor, as well as updraft gasifier this system is used for small-scale applications.

Fluidized-bed gasifier
Biomass is reduced to fine particle size and flowed in the bottom of the reactor. Likewise, high speed oxygen and vapor is flowed undernead the biomass, forcing it to flow upwards through a heated bed of sand and char. Fuel particles lose moisture and

pyrolyse rapidly, sand acts as abrasive removing ash from fuel particle, the tar yield is relatively low (10 g/Nm3) [29]. This system is used for large-scale applications.
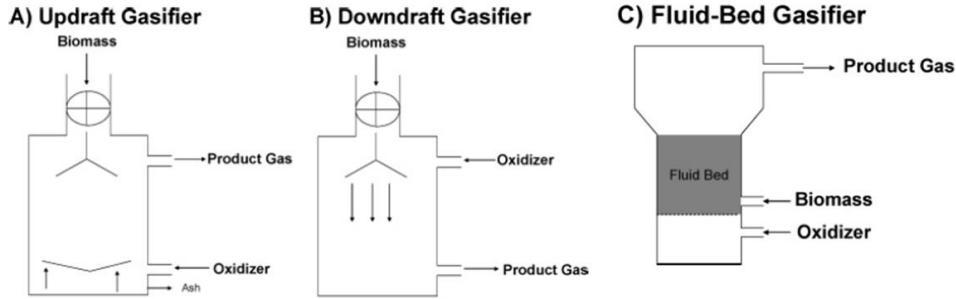
Figure 1.4.- Gassification reactor design.

The stoichiometry of gasification process is presented in the set of **equations A**, in which cellulose is thermal discomposed in the presence of H_2O and O_2. The main reaction products will be H_2, CO_2, H_2O, CO and CH_4. According to the total energy balance, the overall reaction in the gasification process becomes an exothermic process, which leading to seize the energy produced to supply the high amount of heat needed to crack and reform the molecules of H_2O and CH_4 in the succeeding process.

Stoichiometrical Reactions		ΔH(kJ/mol)	
$C_6H_{12}O_5$ ⟶	$5CO + 5H_2 + C$	180	**(A1)**
$C_6H_{12}O_5$ ⟶	$5CO + CH_4 + 3H_2$	300	**(A2)**
$C_6H_{12}O_5$ ⟶	$3CO + CO_2 + 2CH_4 + H_2$	-142	**(A3)**
$C_6H_{12}O_5 + ½ O_2$ ⟶	$6CO + 5H_2$	71	**(A4)**
$C_6H_{12}O_5 + O_2$ ⟶	$5O + CO_2 + 5H_2$	-213	**(A5)**
$C_6H_{12}O_5 + 2O_2$ ⟶	$3CO + 3CO_2 + 5H_2$	-778	**(A6)**
$C_6H_{12}O_5 + H_2O$ ⟶	$6CO + 6H_2$	310	**(A7)**
$C_6H_{12}O_5 + 3H_2O$ ⟶	$4CO + 2CO_2 + 8H_2$	230	**(A8)**
$C_6H_{12}O_5 + 7H_2O$ ⟶	$6CO_2 + 12H_2$	64	**(A9)**
$CO + H_2O$ ⟷	$6CO_2 + H_2$	-41	**(A10)**
$CO + 3H2$ ⟷	$CH_4 + H_2O$	-206	**(A11)**

The overall composition of the gasification outlet will present very small traces of undesired compound, such as tar .13% (dry basis) and H_2S .04% mol (dry basis) [25]. This last one will represent a significant treat for the lifetime and performance of the catalytic processes. In order to avoid the catalyst poisoning it is important to add a pretreatment stage, following the example pathway displayed in **figure 1.3**, calcined dolomite is used as a sorbent agent for the removal of CO_2 (which can cause coke formation at the reforming process due to the excess of C) and H_2S. H_2S sorbion stoichiometry reaction is presented in **equation B**.

2 [CaCO$_3$+MgO] + H$_2$S = [CaS+MgO] + H$_2$O + CO$_2$ **(B)**

Worth mention that this is not the unique technique for H$_2$S removal, but it is an accurate one for low H$_2$S concentrations.

1.2.1.2 Steam Reforming

Hydrogen is mainly produced by the endothermic reaction of CH$_4$ and H$_2$O, the stoichiometry of gasification process is presented in the set of **equations C**. In order to avoid the carbon formation steam/carbon ratio is higher than stoichiometric, for hydrogen process the recommended loading in the feed is a S/C ratio of 2.5.
From a thermodynamic point of view steam reforming depends on process conditions, CO$_2$ favoured by low temperature while CO and H2 at equilibrium is favoured by high temperatures.

Stoichiometrical Reactions	ΔH(kJ/mol)	
CH$_4$ + H$_2$O $\longrightarrow$ CO + 3H$_2$	260	**(C1)**
CO + H$_2$O $\longrightarrow$ CO$_2$ + H$_2$	-41	**(C2)**
CH$_4$ + CO$_2$ $\longrightarrow$ 2CO + 2H$_2$	247	**(C3)**
CH$_4$ $\longrightarrow$ C + 2H$_2$	75	**(C4)**
2CO$_2$ $\longrightarrow$ C + CO$_2$	-173	**(C5)**

To boost H2 production, steam reforming will be followed by water gas shift reaction.

1.2.1.3 Water Gas Shift

In order to increase the production rate of Hidrogen, water-gas shift reaction is used, regarding the exothermic equation D, this process converts the mixture of steam and carbon monoxide into carbon dioxide and more hydrogen. Concerning that the reaction is moderately exothermic, the process is held in an adiabatic reactor.

$$CO + H_2O \longleftrightarrow 6CO_2 + H_2 \qquad \overset{\Delta H}{-41}\textbf{(kJ/mol)} \qquad \textbf{(D)}$$
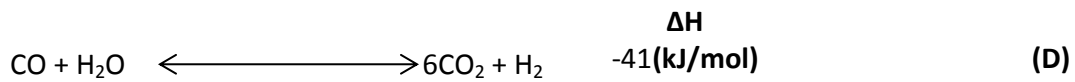
According to the **figure 1.5**, equilibrium constant is thermodynamically favored at low temperatures, the equilibrium constant and CO conversion decreases upon temperature increment, however equilibrium is kinetically limited.
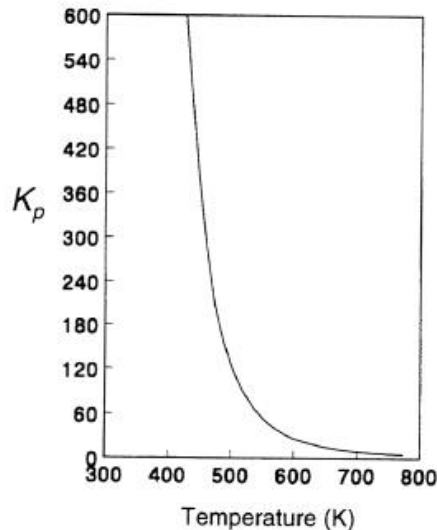
Figure 1.5.- the temperature effect is given by the formula $K = \exp(\frac{4577.8}{T} - 4.33)$ [19]

Due to the invariance in the number of moles during the course of the reaction, pressure effect has a negligible function during WGS equilibrium.

For the purpose of a higher yield, the process is executed in two sequential reactors, the first kinetically favored at high temperature and the second thermodynamically favored at low temperature.

The first stage is called high temperature shift, where temperature is operated between 300°C and 500°C and is run over a chromium or copper promoted iron-based catalysts [31]. The main purpose of this unit is to increase the production rate of hydrogen up to 75 mol% while reducing the CO concentration up to 3 mol% [31], high temperature will favors fast CO consumption and minimizing catalyst bed volume.

In terms of low temperature shift, operating temperature is executed between 210 - 250°C over a copper-zinc-aluminum catalyst bed [30], the carbon monoxide concentration will tend to decrease up to 0.3 mol% [30].

Besides temperature, water will also plays determining role during the WGS conversion, this effect is presented in **figure 1.6**. The increment in the molar S/G ratio will improve the CO equilibrium conversion, especially above 150◦C. The amount of water added to SR and WGS stages must be balanced taking into account the steam production expenses and operating design conditions.
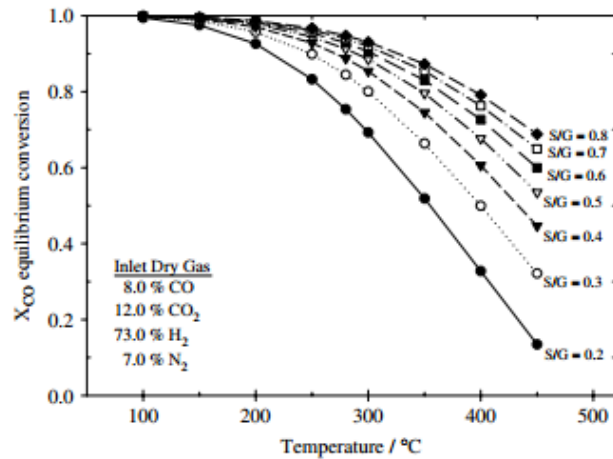
Figure 1.6.- CO equilibrium conversion of a typical reformate steam from a methane steam refrming process at various steam to dry gas (S/G) ratio [32]

1.3 Water gas shift catalyst

According to process requirements, two different catalysts are used for both HTS and LTS. As seen in **figure 1.7** typical catalyst composition will be a significant factor for CO conversion.

The commercial HTS iron-based catalyst is unsupported and has a composition ranging Fe_2O_3 (80–95%), Cr_2O_3 (5–15%), and CuO (1–5%). The Cr_2O_3 additive acts as a stabilizer preventing high temperature sintering, while Cu promoter reduces S/C ratio upto a range of 20% [33]. Prior to the reaction, Fe_2O_3 must be reduced to Fe_3O_4, which is thought to be the active component of the ferrochrome catalyst, the reduction is held upon a mixture of air and an inert gas at a temperatures of 250–400∘C.

In the other hand, the commercial LTS Cu-based has a composition of Cu (51%), ZnO (31%) and Al_2O_3 (18%)[33].Activation requires the reduction of CuO to Cu, which is done by heating up the catalyst below 230°C, to avoid sintering, while a carrier gas (nitrogen or natural gas) and small amount of hydrogen passes through it.
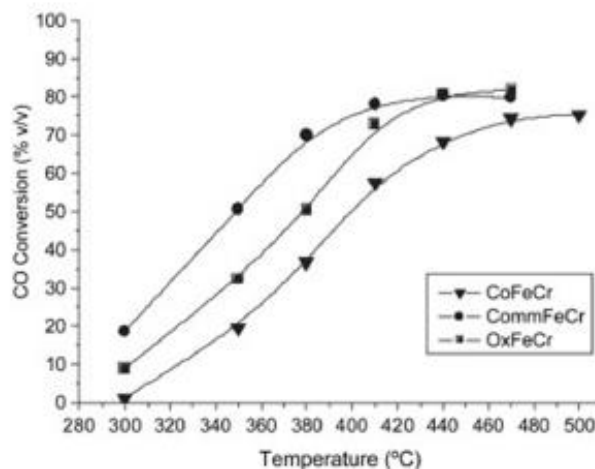
Figure 1.7.- Different performance of FeCr catalyst at HTS; where commercial catalyst has shown to be the more active

Under the purpose of the study, nickel and cobalt were analyzed as potential precursors for WGS reaction, similarly hydrotalcite as the metal support.

1.3.1 Ni base catalyst for WGS

Ni-based catalysts are known for its high performance at the steam reforming process; this is triggered due to its high heat-conductivity that facilitates heat control, it also has been recognized as an alternative catalyst for WGS[34].

Unfortunately, as shown in **equation E** at temp between 250 and 400C Ni based catalyst is an effective precursor for methanation

$$CO + 3H_2 \xleftrightarrow{\hspace{4cm}} CH_4 + H_2O \qquad \overset{\Delta H}{-206}\textbf{(kJ/mol)} \qquad \textbf{(E)}$$
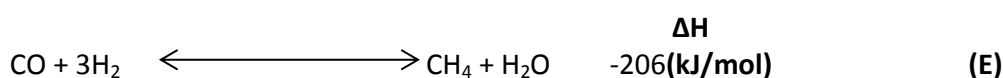
However, it has been shown that the impregnation of Ni-base catalyst with K can promote the activity for WGS and decrease the methanation selectivity[34].The comparison for the performance of this catalyst is displayed in **figure 1.8.**
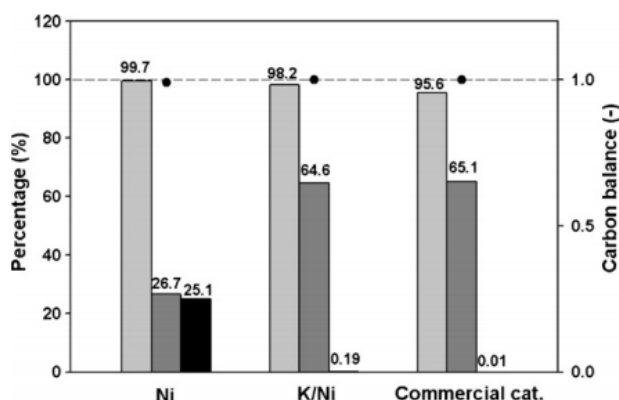
Figure 1.8.- Comparison of three different catalysts for WGS reaction at 350◦C and GHSV of 4000 h−1. Gray bar: CO conversion (%); dark gray bar: H2 production (%); black bar: CH4 production (%); black dot: carbon balance (–)[34].

1.3.2 Co base catalyst for WGS

Cobalt is a highly active WGS catalyst, however, it is unstable and can produce significant by-product hydrocarbon formation due to CO hydrogenation.

Transition metal carbides, such as CoMo carbide, have shown a high activity for the WGS reaction and good oxidation stability [35] but they are easily deactivated in the presence of sulfur. To reduce deactivation, the addition of alkali metals such as K and Zn, has shown an increased on conversion due to the better coke resistance, especially for K [35].

Moreover, it has been shown that a stable CoCr2O4 catalyst promotes high activity and improved sulphur resistance for WGS reaction. [36]

1.3.3 Hydrotalcite

The support determines the dispersion of the active metal particles, strong interaction between metal and support can do a better resistant catalyst to sintering and coking. Also they can participate as an oxidizing or reducing reaction intermediates.

Hydrotalcite-like material offers potential abilities as catalyst supports, this due to its shape recognition for guest materials. Among its advantages are:

- Anion exchange ability in the interlayer.
- Cation exchange ability in the Brucite-like layer.
- Basicity due to their surface hydroxyl functions.

This will give a high activity, selectivity, stability and homogeneous mixture of metal oxides [8-9].

Hydrotalcite compounds are characterized by the following formula:

$$M1_{-x}{}^{2+}Mx{}^{3+}(OH)_2(A^{n-1})_{x/n} \, X \, mH2O$$
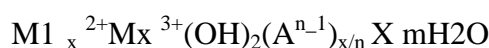
Where M^{2+} is a divalent cation (Mg^{2+}, Ni^{2+}, Co^{2+}), M^{3+} is a trivalent cation (Al^{3+}), and Am_{-} is an interlayer anion ($CO_3{}^{2-}$, OH^{-}). The value of x is typically in the range of 0.20–0.33

As seen in **figure 1.8**, hydrotalcity structure is divided into metal ions and anions layers. Metal ion layer has the Brucite structure, $Mg(OH)2$, interaction between divalent and trivalent ions induces a net positive charge which is occupied by an anion layer charge. The space left by the anion molecule will be filled with water.
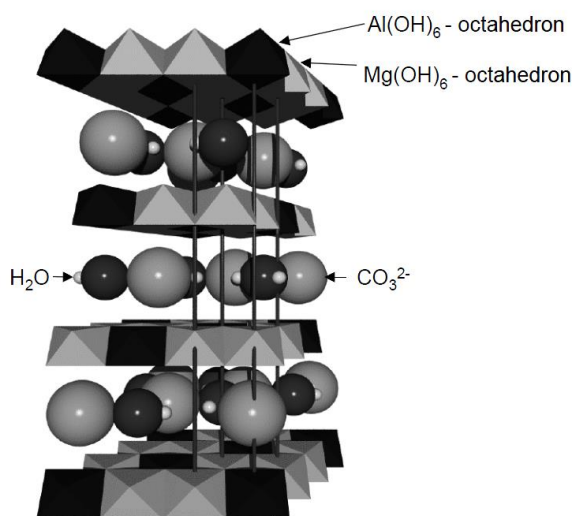
Figure 1.8.- Hydrotalcite Structure [10]

As examples, Ce-promoted Ni-catalysts from HT[37] and Ni on HT [38] like materials were used for methane reforming, as a result, they demonstrated high methane conversion; even, Ni-HT was compared with $NiAl_2O_3$ support, revealing a better performance under severe temperature conditions.

1.3.4 Noble metals

Most of the recent studies have been directed in using any of the precious metals like Pt, Rh, Pd and Au deposited on Ceria, Zirconia, Alumina, Titania, Thoria or Magnesia supports. Besides it affinity for WGS reaction they also promoted the suppression of methanation [39].

Grenoble et al. [40] studied the relationship between the activity of the metal catalyst by means of the strength of interaction between the CO and the surface of pure metal **(Figure 1.9).** CO-M interaction will be proportional to the heat of absorption, for metals that absorb CO weakly the activity will be low, nevertheless if the CO-metal interaction is very strong the CO-M intermediate becomes stable and hence reaction production becomes slow.
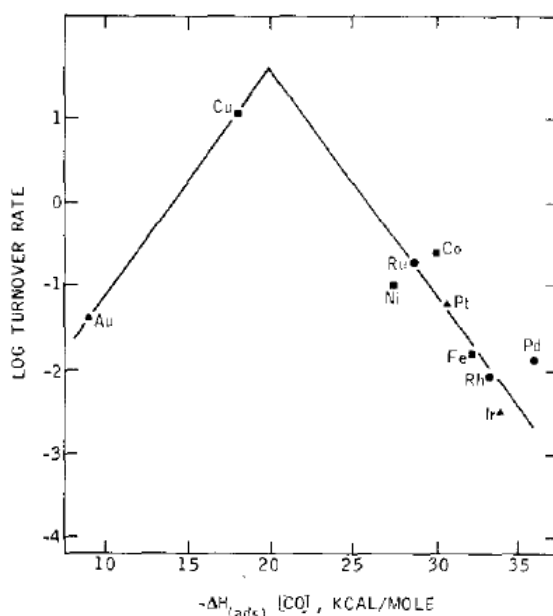
Fig 1.9.- Volcano-shaped relationship between metal turnover number at 300C and heat of adsoption of carbon monoxide.

However, as shown in **figure 1.10,** an experiment performed between Pt containing catalyst against conventional Cu-base catalyst demonstrate that JM8 (Johnson Matthey Pt-containing catalyst) and to Pt–CeO$_2$ WGS catalysts are more active than CuZnO-Al$_2$O$_3$ at intermediate temperature range, enhancing CO conversion and decreasing Methanation.
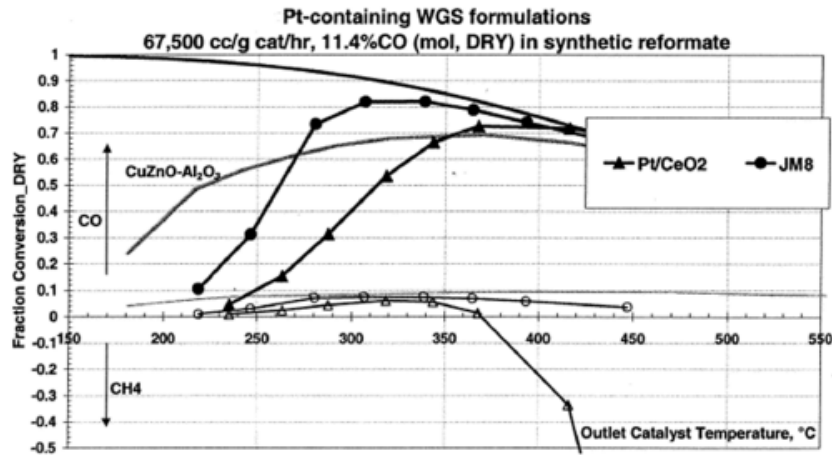
Figure 1.10.- Performance of a Johnson Matthey Pt-containing WGS catalyst compared to Pt–CeO2 at the same metallization, synthetic reformate containing 11.4% CO (mol DRY) [48]

Likewise, J. Wagner at al. [41] compared the effect of different Ce supported metallic catalysts for WGS reaction, demonstrating a higher activity from Pd/ceria and Ni/ceria than either Co/ceria or Fe/ceria.

1.4 Sorption Enhance Techniques

The in-situ removal of CO2 during WGS and SR has shown a positive enhance during the production of H2[33-6, 10-11]. This method has been performed by packing a mixture of a CO2 adsorbent and a WGS/SR catalyst in a single unit.

According to Le Chatelier's principle, if partial pressure of CO_2 descreases as soon as it is formed, the CH_4 reforming and water-gas shift reactions can proceed beyond the conventional thermodynamic limits increasing a higher yield in H2.

The overall reaction occurring are expressed in the set **equitions F**. Equations 1 and 2 represent, respectively, SEWGS and SESR reactions

Stoichiometrical Reactions		ΔH (kJ/mol)	
$CO + H_2O + CaO \longrightarrow CaCO_3 + 5H_2$		-178	**(F1)**
$CH_4 + H_2O + CaO \longrightarrow CaCO_3 + 4H_2$		-12.9	**(F2)**
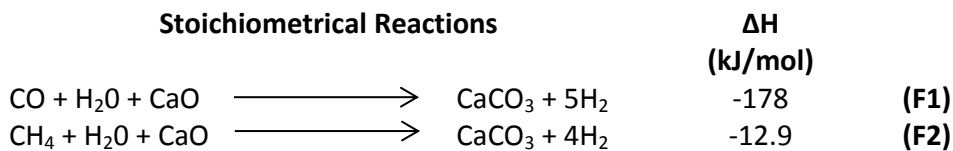
According to the adsorption capacity, kinetical performance for absorption and desorption, thermal stability, availability and cost, calcium carbonate has proved to be an excellent material for CO2 adsorption. [1-6, 17].

The stoichiometry for a CO2 soption reaction is presented in **equation G.**

$$CaO_{(S)} + CO_2 \longrightarrow CaCO_{3(S)} \qquad \textbf{(G)}$$

Grace Jr et al. [42] demonstrate that dolomite has a better mechanical integrity in thermal cycling operation than limestone

Following the above reactions Calcium carbonate must be regenerated after a time on stream. The schematic representation of this process is shown in **figure 1.11**, in which the SESR process will be integraded for two reactors. All three reactions, **F1, F2 and F3,** will be held in this first reactor, which has been previously loaded with a mixture of based reforming catalyst and Ca-based CO_2 sorbent.

The second reactor is used as a thermal regenerator; CO_2 will be removed from the sorbent catalyst either under hot air stream or other inexpensive gas.
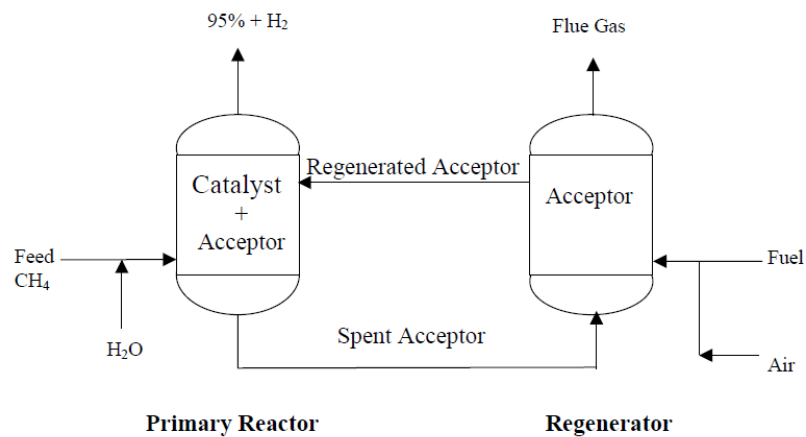
Figure 1.11.- schematic representation a SESR process unit

1.5 WGS rate expression mechanisms

The kinetic rate expressions are important parameter during process design; they are a crucial part for the development and improvement of reactors.

The evaluation of HTS process involves the study of methanation and WGS reactions.

WGSR mechanism over the metal oxide catalyst has been broadly classified as regenerative and associative mechanism, also known, respectively, as redox and carboxyl mechanism.

Redox mechanism is based on water dissociation at the catalyst surface, to produce H_2; meanwhile oxygen at the surface will react with CO to produce carbon dioxide [43]

Redox Mechanism			
CO + *	$\longleftrightarrow$	CO*	1
H2O + *	$\longleftrightarrow$	H2O*	2
H2O* + *	$\longleftrightarrow$	OH* + H*	3
OH* + *	$\longleftrightarrow$	O* + H*	4
CO* + O*	$\longleftrightarrow$	CO2* + *	5
CO2*	$\longleftrightarrow$	CO2 + *	6
2H*	$\longleftrightarrow$	H2 + 2*	7
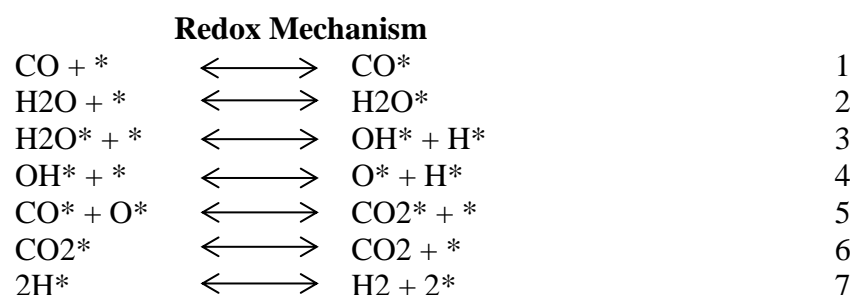
The carboxyl mechanism is an adsorption - desorption model where water is dissociated into H_2 and $OH(-)$. The hydroxyl molecule will interact with the absorbed CO forming a carboxyl intermediate in the surface which then decomposes to form H_2 and CO_2.

Carboxyl Mechanism

CO + * $\longleftrightarrow$ CO*	1
H2O + * $\longleftrightarrow$ H2O*	2
H2O* + * $\longleftrightarrow$ OH* + H*	3
CO* + OH* $\longleftrightarrow$ COOH* + *	4
COOH* + * $\longleftrightarrow$ H* +CO2*	5
CO2* $\longleftrightarrow$ CO2 + *	6
2H* $\longleftrightarrow$ H2 + 2*	7
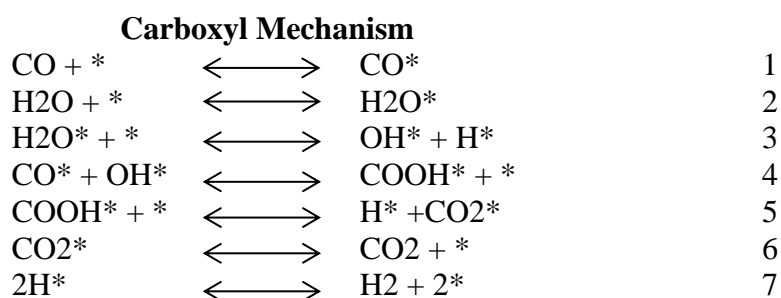
The redox mechanism is normaly used to explain the high temperature water gas shift reaction. Whereas, low temperature water gas shift has been explained using both mechanisms.

Methanation mechanism was proposed by Kelley at al. neglect CO_2 formation, considering that the amount produced was about 2% of the CH_4. Nevertheless, according to the main approach of this project, consider this mechanism would be erroneous. In the other hand Iglesias et al. suggested two possible pathways for the chain growth, (based in Fischer–Tropsch over a Fe catalyst) either H-assisted and unassisted routes

Unassisted CO dissociation

CO + * $\longleftrightarrow$ CO*
H2 + 2* $\longleftrightarrow$ 2H*
CO* + * $\longleftrightarrow$ C* + O*
C* + H* $\longleftrightarrow$ CH* + *
CO* + O* $\longleftrightarrow$ CO2* + 2*
CH* + H* $\longleftrightarrow$ CH2* + *
CH2* + H* $\longleftrightarrow$ CH3* + *
CH3* + H* $\longleftrightarrow$ CH4 + 2*

H-assisted CO dissociation

CO + * $\longleftrightarrow$ CO*
H2 + 2* $\longleftrightarrow$ 2H*
CO* + H * $\longleftrightarrow$ HCO* + *
HCO* + H* $\longleftrightarrow$ HCOH* + *
HCOH* + * $\longleftrightarrow$ CH* + OH*
OH* + H* $\longleftrightarrow$ H2O + 2*
CH* + H* $\longleftrightarrow$ CH2* + *
CH2* + H* $\longleftrightarrow$ CH3* + *
CH3* + H* $\longleftrightarrow$ CH4 + 2*
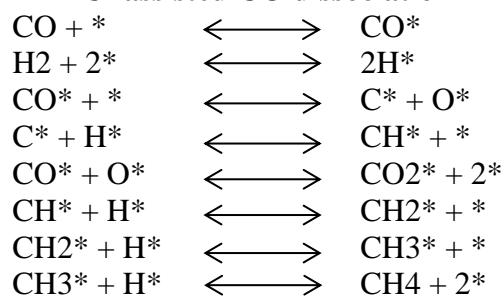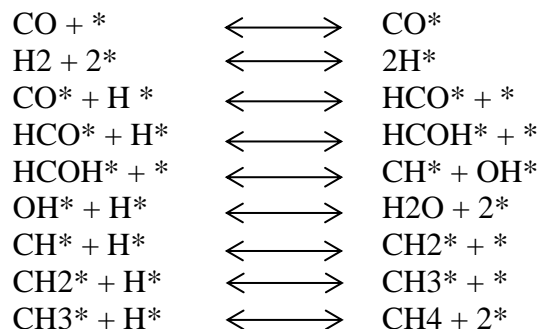
Several authors have obtained different ranges of kinetic expressions, most of the works confirm to the power law rate expression for kinetic equilibrium. Reverse WGS is used as an approach to balance the reaction equilibrium.

Base on literature review, **table 1**[40,44,45] summarizes a list of kinetic data achieved using noble metal in the WGS reaction.

Catalyst	Operating Conditions	Arrehnius Parameter		Reaction Order			
		Ko	Ea	L (CO)	m (H2O)	q (CO2)	p (H2)
Ru	30 0℃-	1.5×10^7	80	-	-	-	-
Ru/ceria	1000℃ .008	5.0×10^7	80	-	-	-	-
Ni	to.05s	8.0×10^7	85	-	-	-	-
Ni/ceria	contact	1.7×10^8	85	-	-	-	-
Rh	time coated	3.0×10^9	130	-	-	-	-
Rh/Ceria	on lumina	1.5×10^{10}	130	-	-	-	-
Pd	support	4.0×10^6	100	-	-	-	-
Pd/Ceria	5wt%	4.0×10^7	100	-	-	-	-
Pt	loading	1.0×10^6	80	-	-	-	-
Pt/Ceria		2.5×10^7	80	-	-	-	-
Rh/ Al_2O_3	330 ˚C	5.1×10^6 molecules/s/site	96 ± 5	-.1	-.44		
Rh/SiO_2	350	3.23×10^5 molecules/s/site	95 ± 10	-.24	.53	-	-
1%Pt/Al_2O_3	1atm,225 ˚C – 285 ˚C		68	.1	1.1	-.07	.44
1%Pt/Al_2O_3	1atm,2850C – 345 ˚C		84	.06	1	-.09	-.44
1.66%Pt/Al_2O_3	1atm,285 ˚C		81	.11	.82		
1.66%Pt/Al_2O_3	1atm,300 ˚C		82	-.21	.75	-	-
.9% Pt/Al_2O_3	1atm,100 ˚C			.02	.55	-	-.22

Catalyst	Conditions	Rate constant	E_a	l	m	n	q
.4%Pt/ Al_2O_3	1atm,5440C		39	.45	.37	0	-.73
Pt/ Al_2O_3	270 ˚C	1.9×10^6 molecules/s/site	82 ± 5	-.21	.75	-	-
1%Pt/CeO_2	1 atm 200 ˚C	-	75	-.03	.44	-.09	.38
1%Pt/CeO_2	1 atm 240 ˚C		46	0	1	-	-
1%Pt/CeO_2	-		91	.14	.66	-.54	-.08
Pt/SiO_2	340 ˚C	1.18×10^5 molecules/s/site	80 ± 53	-.08	.69	-	-
Pt/C	340 ˚C	3.84×10^6 molecules/s/site	107± 6	.13	.35	-	
1%Pt/TiO_2	-	-	59	.3	.85	-.67	0
1.4%Pt – 8.3% CeO_2/ Al_2O_3	1 atm 260 ˚C	-	86	.13	.49	-.12	-.45
2% Pt/ 1% Re/CeO2-ZrO2	1 atm 210 ˚C - 260 ˚C	-	71	-.05	-.32	.85	-.05
CuO.2Ce.8O2-y (CU-ceria)	100 ˚C - 350˚C CO/H2O= .33	1.8×10^3	61	-	-	-	-

Table 1: Reaction orders and activation energy for different noble metal catalysts

Power law rate expression is given by

$$r = kP^l_{CO}P^m_{H2O}P^n_{CO2} P^q_{H2} (1 - \beta)$$

Where rate constant k is expressed as

$$k = K_o^{\left(-\frac{E_a}{RT}\right)}$$

Ko is preexponential or frequency factor, Ea is activation energy and β is the approach to equilibrium and is given by

$$\beta = \frac{P_{CO2} P_{H2}}{K_{eq}P_{CO}P_{H2O}}$$

Whether β is higher than .2 it means that the reaction is not at thermodynamic equilibrium. As indicated in the chapter 1.2.3.1, Keq is the equilibrium constant.

2. Experimental

Co–Ni Catalyst derived from Hydrotalcite-Like material was prepared by co-precipitation; in addition small traces of Pd with different concentrations were deposited via surface redox reaction.

The different compositions during for the catalyst preparation is given in **appendix A**. In the same manner Pd dissolution calculations are provided in **appendix B**.

2.1 Catalytic preparation

HT-derived Ni-Co catalyst was prepared stoichiometrically under a fixed metal loading of 20% Ni and 20% Co.

A homogeneous cation solution of $Co(NO_3)2.6H_2O$, $Ni(NO_3)2.6H_2O$, $Mg(NO_3)2.H_2O$ and $Al(NO_3)_3.9H_2O$ was diluted in 400 ml of deionized water into a three- necked reactor flask. An anion solution of NaOH and Na_2CO_3 was prepared and diluted homogenously in 400ml of deionized water in an Erlenmeyer flask. This mixture was pumped drop by drop to the cationic solution with an average flow of 200 ml/h.

Once the solution has been homogenized, the pH is adjusted to 8.5 using HNO. Finally, the mixture is refluxed to 80ºC during 12 hours aging time. The resulting slurry is washed and filtered with deionized water, until it reaches a pH in the range of 7.4, The catalyst is then dried and calcined at 600 ºC for 6 hrs. with an increasing heating rate of 5 ºC/min.

In order to achieve the Palladium surface redox reaction, the catalyst must be reduced under a molar flow of N_2 and H_2 at 650 ºC for 11 hr. with an increasing heat of º5 C/min. Once the Ni-Co HT catalyst has been reduced the reactor is cooled. All the H_2 must be removed in order to have an inert atmosphere inside the reactor.

In the meantime, the cation solution $Pd(NO_3)_2 \cdot 2H_2O$ is diluted with deionized water and heated up to 80ºC over 12 hrs.

The deposition of Pd^{2+} ions into the reduced Ni-Co HT catalyst is done via a redox reaction at inert atmosphere

Picture 2.1 .- Pd surface redox setup

Equation H1 & H2 describe the overall redox reactions as it supposed to occur.

$$Ni(s) + Pd^{2+} (aq) \rightarrow Ni^{2+} (aq) + Pd(s) \qquad \textbf{(H1)}$$

$$Co(s) + Pd^{2+} (aq) \rightarrow Co^{2+} (aq) + Pd(s) \qquad \textbf{(H2)}$$
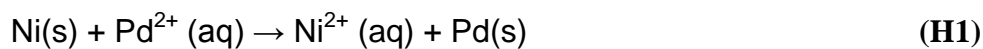
As shown in **picture 2.1,** Pd solution is pumped at the top of the reactor flowing downstream the catalytic bed. Once the Pd solution has been reduced (solution use to crystalline), the reactor is removed, and the catalyst is dried during 12 hrs, finally the catalyst is calcined at 600°C for 5 h with a heating increase of 5°C/min

All catalyst were prepared in same manner, different compositions regarding Pd percentages are summarized in table 2

Sample	Composition			
Pd %	Ni (%)	Co (%)	Pd (%)	HT Base (%)
0	20.00	20.00	0	60.00
25.00	19,69	19,69	1,545	59,07
50.00	19,39	19,39	3,044	58,17
75.00	19,10	19,10	4,498	57,30

Table 2. - Pd/Ni-CO HT Partial Composition.

2.2 Characterization

Characterization was done using X-ray Diffraction and Chemisorption techniques. All procedures were followed at NTNU.

2.2.1 XRD

Metal dispersion was calculated using a AXS D8 Focus unit.

The structural analyst is obtained from the average diffraction of an X-ray beam projected through a particle lattice over an angular range of 90º at a scan speed of 2˚/min with and increment of .02

All graphic peaks were analyzed with EVA software version.

2.2.2 Chemisorption

The Metal dispersion was calculated by hydrogen chemisoption isotherms in a quart micro-reactor, using the Micrometrics ASAP 2010 unit by means of static chemisorption principle.

Samples were calcined before starting the insitu reduction for chemisorption.

Once the catalyst has being reduced, a known volumetric quantity of gas (H2) is gradually dose into the quartz reactor. When the reactor content has reached the equilibrium, the number of H_2 moles adsorbed is measured concerning the decrease in pressure of the system. This measure is repeated, but increasing the pressure of the gas until equilibrium.
Once the second trial is finished, the volume (Y axis) and Pressure (X axis) isotherms are plotted, the difference between the two isotherms represent the chemisorbed amount of H_2.

Dispersion can be calculated with the **formula 1**. Where **V**$_{ads}$ is the gas adsorbed over an average atomic weight; this one is represented by **$\dot{M}$.**

$$D(\%) = \frac{Vads \; x \; \dot{M}}{E \; x \; W} \; X \; 100 \qquad (1)$$

E regards to the ration among the adsorbed gas molecules per metal particles, and W is the fraction of metal in the catalyst.

2.3 Reaction order and SE experiments

All experiments were carried out in the "Microactivity reference reactor" SPANSK I, located at Chemistry hall, at the Chemical Engineering Department, NTNU.

Previous experiments all catalyst was pelletized, ground and sieved to 250-500 µm particle size.

2.3.1 Set up description

As can be appreciated in **figure 2.2**, the SESR setup present 3 Bronkhorst mass flow controllers, that are integrated directly both to the control panel and the digital remote control system (desktop computer). Additional mass flow controllers can be connected to the gas inlet, but they must be locally controlled.

In Additional to the flow controllers, water is introduced with by a Gilson HPLC pump which downstream, is connected to the internal evaporator. The pump is controlled locally in order to dose the specific amount water that will flow downdraft the reactor for its conversion.

Once the gases and steam has been mixed, they flow through a six way valve; whether the valve is set at the by-pass position, gases will flow toward the outlet directly to the ventilation fume, without having any contact with the catalytic bed. If the by-pass position is deactivated, the gases will flow through the reactor. After the reaction has been made, gases are cooled down by means of a condenser (Peltier) integrated in the MA unit. The water that hasn't been drained out will be condensed with the addition of a cold trap. Finally a portion of gases will flow through the Agilent 3000 Micro GC, that will measure the mole fraction composition of the product gas.
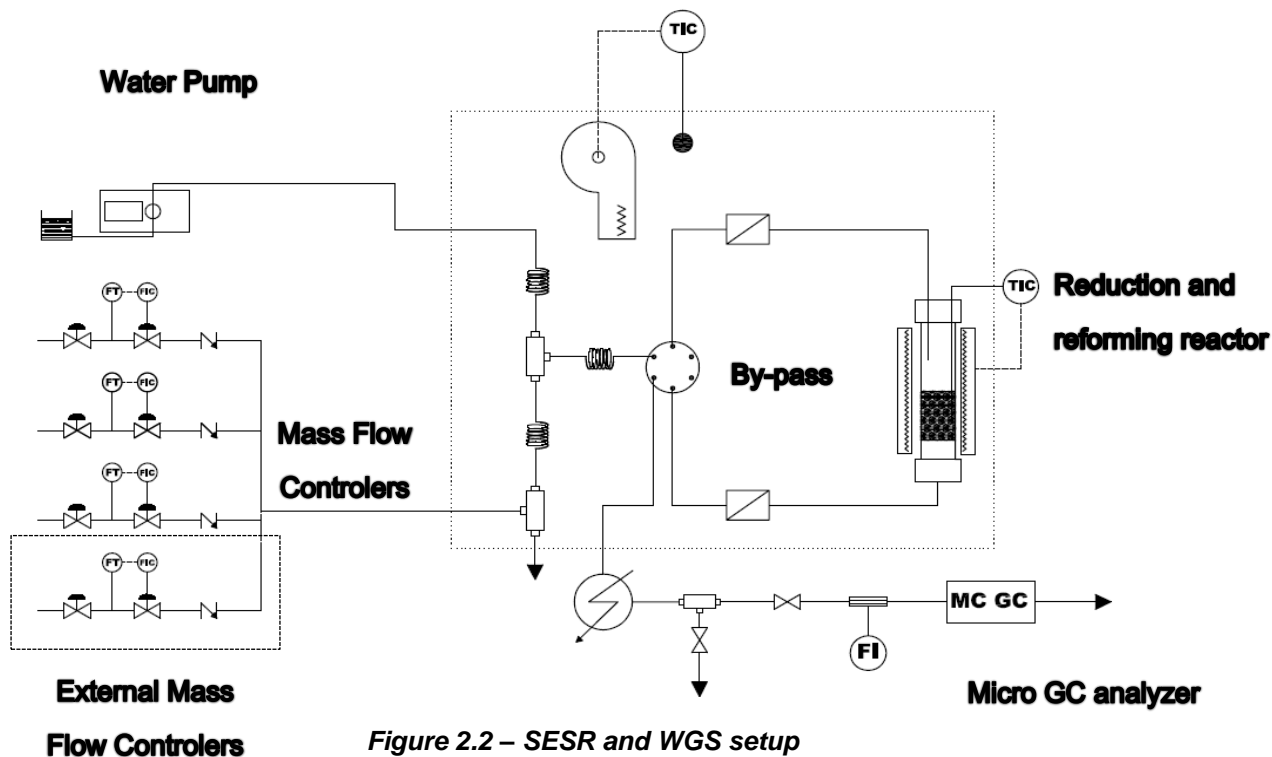
Figure 2.2 – SESR and WGS setup

2.3.2 Experimental procedure

Kinetic and SEWGS experiment were held in different quartz reactors, as seen in **figure 2.3** kinetic experiments were performed in tubular fix bed reactor of 8mmØ x 19.25 cm with a volume of 38.704 cm^3, in the other hand sorption enhance experiments were performed in a 14.5mmØ x 19.5 cm tubular fix bed reactor with a volume of 128.801 cm^3
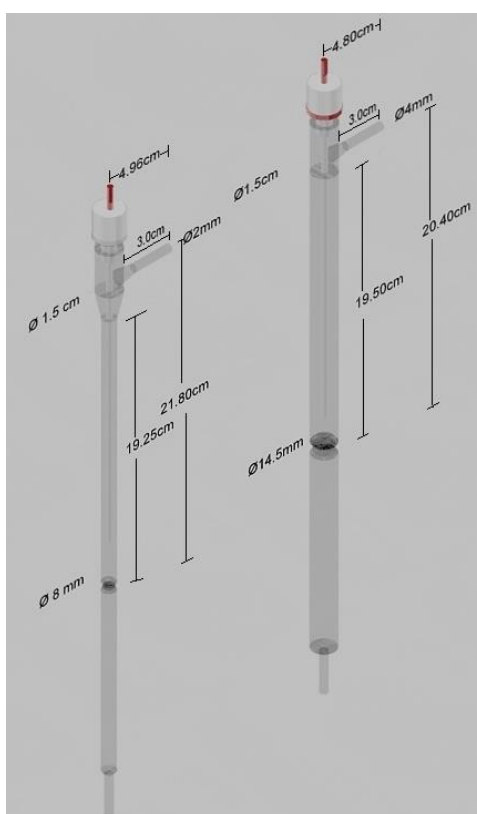
Figure 2.3.- 5:1 scale representation of the quartz reactors. Left hand side belongs to the kinetic reactor whereas left hand represents the sorption enhance reactor model.

Inside the reactor there is a capillary tube, which is used to place a thermocouple; this one will sense the temperature in which the reaction is occurring. All experiments were drove in the set-up exposed in chapter 2.3.1

2.3.2.1 Experimental kinetic study

The catalytic bed was prepared with a mixture of 4.8 mg of catalyst and 40 mg of of α-Al$_2$O$_3$ supported and packaged over a fine base of alumina wool.
When the reactor is ready, we proceed to perform the leak test followed by the reduction of the catalyst; this one is carried out with a mixed gas flow of H$_2$ and He at 620℃ for 10 hrs with an increasing heating rate of 10 ℃/min.
After the reduction has finished the catalyst is cooled down to the temperature conditions of the experiment and the H$_2$ remnant is dragged out with He.

Once the temperature has reached the set point, the six-way valve is turned into the by-pass position and letting all the other gases to flow inside the setup. It is important to let the gases flow over 10 minutes, in order to stabilize the mass flow controllers. To

ensure any deviation in the gas supply the known flows are measured by the micro GC analyzer. Finally the by-pass is turned off and the experiment is carried on.

All kinetic experiments were performed in a low convertion regimen to avoid the influence of the forward reaction, the different gas concentrations according to diverse experimental ratios are presented in the **tables F1a, F1b & F1a in appendix F.**

2.3.2.2 Experimental Sorption Enhance Water Gas Shift

Alike, SEWGS experiments follow the same procedures for leak test and reduction as the kinetic tryouts. In contrast, the catalyst bed was prepared with a mixture of .4 g of catalyst and 4 g of Dolomite sorbent, which were supported and packaged over a fine alumina wool base.

Gas stabilization is executed equally as the procedure described in the kinetic experiment, but unlike, SEWGS is only ran with CO and water to produce WGS reaction, in addition He is used as a carrier gas.

SEWGS reaction occurs when the micro GC analyzer measurements are below equilibrium. Once the CO_2 detected has grown until reaching a steady state, the experiment is concluded, leading to the desorption step; this one is executed by flowing air at 700℃ for 4 hrs. with an increasing heating rate of 15 ℃/min. For the evaluation of these experiments the reaction and regeneration were repeated 7 times on a cyclical manner.

2.4 Calculations

WGS reaction rate is described in formula 2, were XCO represents de convertion , W de mass of the catalyst and F the molar flow of CO. As mention in chapter 1.5, if β is higher than .2 it means that due to the forward reaction the equation is not at thermodynamic equilibrium, in order to correct this, the rate expression will be divided by (1 - β), giving up a new reaction rate **(Formula 3).**

$$r = \frac{dxCO}{d(\frac{W}{Fout})} \qquad (2)$$

$$rf = \frac{r}{(1-\beta)} \qquad (3)$$

Carbon balance will be calculated upon equilibrium from the inlet flows and the molar partial pressures measured by the micro GC analyzer. This mass balance is expressed by **formula 4**, being F_{out} the unknown data. The total CO conversion regards to CO_2 and CH4 formed. As seen in **formula 5 and 6**, respectively, conversion can be calculated between the ratio of the molar flows of product against CO at the inlet,

$$\text{Fin } (YCO + YCO2) = \text{Fout}(Y'CO + Y'CO2 + Y'CH4) \qquad (4.1)$$

$$\text{Fout} = \frac{\text{Fin}(YCO+ YCO2)}{(Y'CO+Y'CO2+ Y'CH4)} \qquad (4.2)$$

$$XCH4 = \frac{\text{Fout} * Y'CH4}{\text{Fin}* YCO} \qquad (5)$$

$$XCO2 = \frac{(\text{Fout}* Y'CO2)-(\text{Fin}* YCO2)}{\text{Fin}* YCO} \qquad (6)$$

Turn over frequency is calculated by dividing the reaction rate under the number of sites, were M is the molar weight of the metal composition, $X_{NI\text{-}CO\text{-}PD}$ is the fraction of the metal loading and D is the metallic dispersion.

$$\text{TOF} = \frac{r*M}{XCo.Pd.Ni* D} \qquad (7)$$

As seen in formula (9), molar flow of CO_2 can be calculated multiplying the mole fraction per total flow-out. According to the different phases in the SEWGS experiments, each cycle can be classified as SEWGS, transition and HTS phase. The aim of the experiment is to calculate how many grams of H2, CO2 and CH4 differ either by increment or inhibition during the SEWGS period against the HTS. Formula 10 will be used for the calculate the mass change; this one is achieved by the differential between SEWGS and Steady State average of CO_2 flow at the outlet, multiplied by both the time on stream (t) and molecular weight the gas.

In order to know the total flow-out, Unisim software was used, simulating the same conditions as the lab experiment. Gibbs reactor is used to simulate the HTS; since unisim provides all Gibbs free energy data for the reactants. After the reactor unit a splitter component was used to separate the dry products of methanation and WGS reactions at equilibrium.

Simulation results can be found in appendix F.

$$Y'_{CO2} * \text{Fout} = F_{CO2} \qquad (8)$$

$$\text{mco} = \big(FCO2(sewgs) - FCO2(ss)\big) * M * t \qquad (9)$$

Same formulas (8 and 9) can be used to calculate de mass and molar flow of CH_4 and H_2.

3. Results

3.1 XRD

The X-ray diffraction testing was made to calcined samples, so as to differentiate the patterns of the Metal-HT presented in **figure 3.1** which belongs to the catalyst calcined about one month before the characterization, on the other hand **figure 3.2** shows the patterns of a freshly calcined catalyst (on the same day of tryout).

Figure 3.1 shows both characteristic diffraction reflections of HT structure and spinel phases. The 2Θ peaks located about 21°, 38°, 44°, 55° and 60° can belong to $CoAl_2O_4$, Co_2AlO_4, $MgCo_2O_4$, $NiCo_2O_4$ and/or Co_3O_4; these oxides have similar XRD patterns. The peak located at 19° belong either Co3O4 or Co, it is also important to mention the growth in 35° peak according to the noble metal content in each sample; this belongs to Pd, same condition occurs in the opposite way relating to Ni and Co oxides, were the 25% Pd content catalyst has the sharpest peaks. Finally, last but not least, the usual HT pattern located at 63°, that probably was re-formed due to the re-hydration of the catalyst. Sample 1% Pd/20Ni-20Co HT has the sharpest HT peak, which is gradually reduced according to the increment in Pd, concluding that this one affects the crystal structure of catalyst.
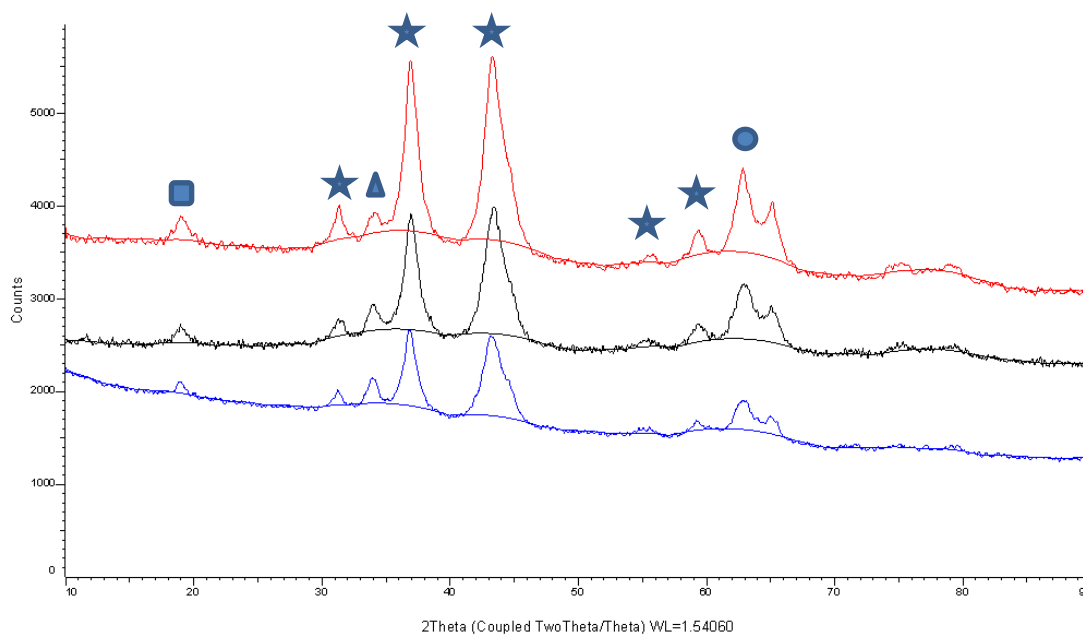
Figure 3.1.- XRD pattern of the "partial hydrated" catalyst, from top to the bottom, 1%Pd/20Ni-20Co HT, 3.0Pd/20Ni-20Co HT, 4.5Pd/20Ni-20Co HT, peaks marked with a ★ are characteristic of $CoAl_2O_4$, Co_2AlO_4, $MgCo_2O_4$, $NiCo_2O_4$ and/or Co_3O_4, the peak marked with a ▢ are caracterised of Co3O4 and Co, the peaks marked with ⬤ and ▲ belongs, respectively, to Pd and a HT structure.

Figure 3.2 shows a vanish in HT pattern, caused by the water removal in the structure, in the same manner Pd 35° peak disappeared, leading to the formation of PdO. This one is not so easy to identify because its spectra overlies with the Ni and Co oxide peaks.
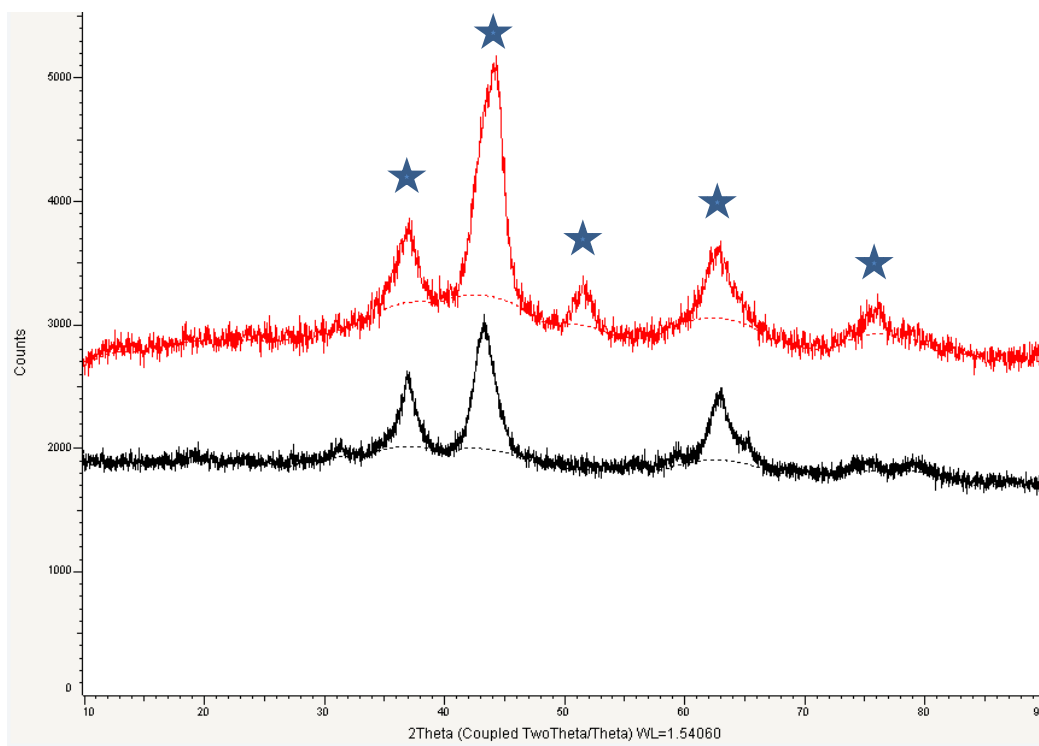
Figure 3.2.- From top to the bottom, 1%Pd/20Ni-20Co HT, 4.5Pd/20Ni-20Co HT XRD pattern of Co$_3$O$_4$, CoAl$_2$O$_4$, NiAl$_2$O$_4$, PdO$_3$, PdO, MgCo$_2$O$_4$, NiCo$_2$O$_4$, Al$_2$MgO$_4$.

3.2 Chemisorption

To calculate the volume of the chemisorbed monolayer (Vm), it is important to identify from the sorption isotherms when the volume of H$_2$ adsorbed has reached the Langmuir model behavior. This means that the development of the isotherm is under equilibrium and it is steadily increasing.

Chemisorbed monolayers corresponding calcined samples 25, 50 and 75 Pd are displayed in **figure 3.3,** were to absorption equilibrium start in the range of 105.
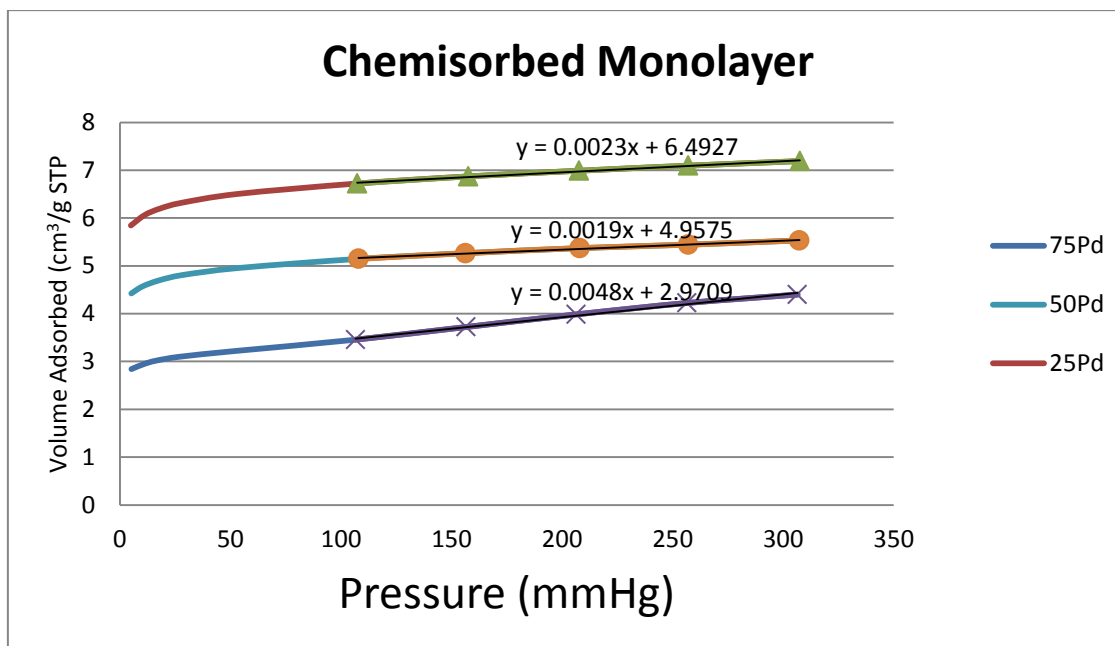
Figure 3.3.- Chemisorbed monolayers from top to the bottom, 1%Pd/20Ni-20Co HT, 3.0Pd/20Ni-20Co HT, 4.5Pd/20Ni-20Co HT

Same characterization was done to the uncalcined 25, 50 and 75 Pd samples, in order to know how does calcination alters the physical properties of the surface. A summary of the data obtained in both, calcined and uncalcined, testing is summarized in **table 3.**

Sample Pd %	Chemisorption results		
	D (%)	*d* (nm)	*Metal surface area* ($m^2_{metal}/g_{catalyst}$)
25 Pd uncalcined	5.9	16.7	15.18
25 Pd calcined	8.6	11.6	21.66
50 Pd uncalcined	5.0	20.0	11.69
50 Pd calcined	6.5	15.4	16.49
75 Pd uncalcined	3.2	30.97	7.45
75 Pd calcined	3.9	25.32	10.39

Table 3.- Diffraction, Diameter and metal surface area, as a results of chemisorption characterization

As seen in **table 3**, for all the catalysts, the dispersion and metal surface area follow the same trend, 25Pd>50>75, alike, low dispersion goes along with a higher crystal size, in the mean that 75Pd reported the highest diameter. Also according to the support property, calcination facilitates the dispersion of metals in the catalyst.

3.3 Water gas shift reaction mechanism

For the porpoise of the study, the two mechanisms proposed in section 1.5 were developed using Langmuir-Hinshelwood model, in addition a COH intermediate and a carbonaceous acid formation –dissociation mechanisms were also proposed and developed.

All Rate determining steps were selected according to the "possible" main reaction in the catalyst surface.

- **Redox mechanism**
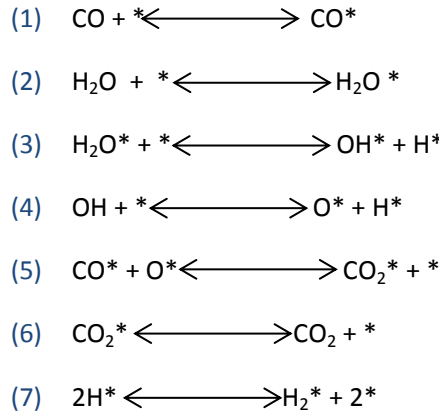
(1) $CO + * \longleftrightarrow CO*$

(2) $H_2O + * \longleftrightarrow H_2O *$

(3) $H_2O* + * \longleftrightarrow OH* + H*$

(4) $OH + * \longleftrightarrow O* + H*$

(5) $CO* + O* \longleftrightarrow CO_2* + *$

(6) $CO_2* \longleftrightarrow CO_2 + *$

(7) $2H* \longleftrightarrow H_2* + 2*$

If step 3 (water dissociation) is the rate determining step:

$$r_3 = \frac{K_3 K_2 P_{H_2O}(1-\beta)}{\left(1 + K_1 P_{CO} + K_2 P_{H_2O} + \frac{P_{CO_2}}{K_6} + \sqrt{\frac{P_{H_2}}{K_7}} + \frac{P_{CO_2}}{K_1 K_5 K_6 P_{CO}} + \frac{P_{CO_2}\sqrt{P_{H_2}}}{K_1 K_4 K_5 K_6 \sqrt{K_7} P_{CO}}\right)^2}$$

If step 4 (OH dissociation) is the rate determining step:

$$r_4 = \frac{K_4 K_2 K_3 \sqrt{K_7} P_{H_2O} P_{H_2}^{-0.5}(1-\beta)}{\left(1 + K_1 P_{CO} + K_2 P_{H_2O} + \frac{P_{CO_2}}{K_6} + \sqrt{\frac{P_{H_2}}{K_7}} + \frac{P_{CO_2}}{K_1 K_5 K_6 P_{CO}} + \frac{K_3 K_2 \sqrt{K_7} P_{H_2O}}{\sqrt{P_{H_2}}}\right)^2}$$

If step 5 (CO2 formation) is the rate determining step:

$$r_5 = \frac{K_5 K_1 K_2 K_3 K_4 K_7 P_{CO} P_{H_2O} P_{H_2}^{-1}(1-\beta)}{\left(1 + K_1 P_{CO} + K_2 P_{H_2O} + \frac{P_{CO_2}}{K_6} + \sqrt{\frac{P_{H_2}}{K_7}} + \frac{K_2 K_3 K_4 K_7 P_{H_2O}}{P_{H_2}} + \frac{K_3 K_2 \sqrt{K_7} P_{H_2O}}{\sqrt{P_{H_2}}}\right)^2}$$

- **Carboxyl mechanism**
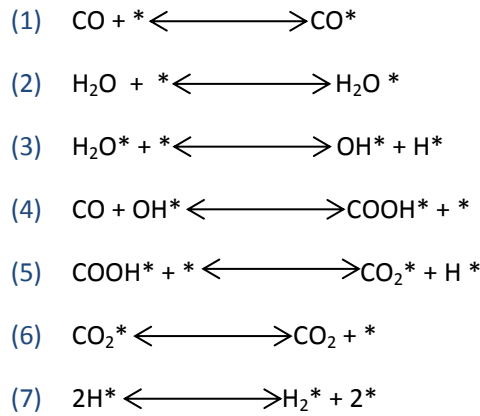
(1) $CO + * \longleftrightarrow CO*$

(2) $H_2O + * \longleftrightarrow H_2O*$

(3) $H_2O* + * \longleftrightarrow OH* + H*$

(4) $CO + OH* \longleftrightarrow COOH* + *$

(5) $COOH* + * \longleftrightarrow CO_2* + H*$

(6) $CO_2* \longleftrightarrow CO_2 + *$

(7) $2H* \longleftrightarrow H_2* + 2*$

If step 3 (water dissociation) is the rate determining step:

$$r_3 = \frac{K_3 K_2 P_{H_2O}(1-\beta)}{\left(1 + K_1 P_{CO} + K_2 P_{H_2O} + \dfrac{P_{CO_2}}{K_6} + \sqrt{\dfrac{P_{H_2}}{K_7}} + \dfrac{P_{CO_2}\sqrt{P_{H_2}}}{K_5 K_6 \sqrt{K_7}} + \dfrac{P_{CO_2}\sqrt{P_{H_2}}}{K_1 K_4 K_5 K_6 \sqrt{K_7} P_{CO}}\right)^2}$$

If step 4 (COOH dissociation) is the rate determining step:

$$r_4 = \frac{K_4 K_1 K_3 K_2 \sqrt{K_7}\, P_{CO} P_{H_2O} P_{H_2}^{-.5}(1-\beta)}{\left(1 + K_1 P_{CO} + K_2 P_{H_2O} + \dfrac{P_{CO_2}}{K_6} + \sqrt{\dfrac{P_{H_2}}{K_7}} + \dfrac{P_{CO_2}\sqrt{P_{H_2}}}{K_5 K_6 \sqrt{K_7}} + \dfrac{K_3 K_2 \sqrt{K_7} P_{H_2O}}{\sqrt{P_{H_2}}}\right)^2}$$

If step 5 (COOH dissociation) is the rate determining step:

$$r_5 = \frac{K_5 K_1 K_3 K_2 K_6 \sqrt{K_7}\, P_{CO} P_{H_2O} P_{H_2}^{-.5}(1-\beta)}{\left(1 + K_1 P_{CO} + K_2 P_{H_2O} + \dfrac{P_{CO_2}}{K_6} + \sqrt{\dfrac{P_{H_2}}{K_7}} + \dfrac{K_1 K_2 K_3 K_6 \sqrt{K_7}\, P_{H_2O} P_{CO}}{\sqrt{P_{H_2}}} + \dfrac{K_3 K_2 \sqrt{K_7} P_{H_2O}}{\sqrt{P_{H_2}}}\right)^2}$$

- **Mechanism involving COH**

(1) $CO + * \longleftrightarrow CO*$

(2) $H_2O + * \longleftrightarrow H_2O*$

(3) $H_2O* + * \longleftrightarrow OH* + H*$

(4) $OH* + * \longleftrightarrow O* + H*$

(5) $CO* + H* \longleftrightarrow COH* + *$

(6) $COH* + O* \longleftrightarrow COOH* + *$

(7) $COOH* + * \longleftrightarrow CO_2* + H*$

(8) $CO_2* \longleftrightarrow CO_2 + *$

(9) $2H* \longleftrightarrow H_2* + 2*$
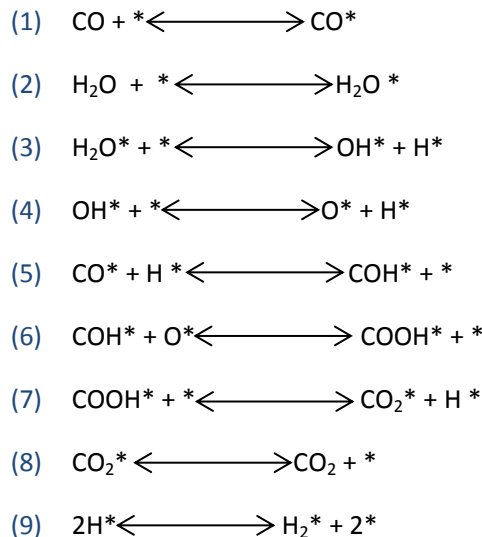
If step 4 (OH dissociation) is the rate determining step:

$$r_4 = \frac{K_4 K_3 K_2 \sqrt{K_9}\, P_{H_2O}\, P_{H_2}^{-.5}(1-\beta)}{\left(1 + K_1 P_{CO} + K_2 P_{H_2O} + \frac{P_{CO_2}}{K_6} + \sqrt{\frac{P_{H_2}}{K_9}} + \frac{P_{CO_2}}{K_1 K_6 K_7 K_8 K_5 P_{CO}} + \frac{K_3 K_2 \sqrt{K_9} P_{H_2O}}{\sqrt{P_{H_2}}} + \frac{K_1 K_5 P_{CO}\sqrt{P_{H_2}}}{\sqrt{K_9}} + \frac{P_{CO_2}\sqrt{P_{H_2}}}{K_8 K_5 K_7 \sqrt{K_9}}\right)^2}$$

If step 5 (COH formation) is the rate determining step:

$$r_5 = \frac{K_5 \dfrac{K_1}{\sqrt{K_9}} P_{CO} P_{H_2}^{.5}(1-\beta)}{\left(1 + K_1 P_{CO} + K_2 P_{H_2O} + \frac{P_{CO_2}}{K_6} + \sqrt{\frac{P_{H_2}}{K_9}} + \frac{K_2 K_3 K_9 K_4 P_{H_2O}}{P_{H_2}} + \frac{K_3 K_2 \sqrt{K_9} P_{H_2O}}{\sqrt{P_{H_2}}} + \frac{P_{CO_2} P_{H_2}\sqrt{P_{H_2}}}{K_2 K_3 K_4 K_6 K_7 K_8 K_9 \sqrt{K_9}\, P_{H_2O}} + \frac{P_{CO_2}\sqrt{P_{H_2}}}{K_8 K_5 K_7 \sqrt{K_9}}\right)^2}$$

If step 6 (COOH formation) is the rate determining step:

$$r_6 = \frac{K_6 K_1 K_5 K_4 K_3 K_2 \sqrt{K_9}\, P_{CO} P_{H_2O}\, P_{H_2}^{-.5}(1-\beta)}{\left(1 + K_1 P_{CO} + K_2 P_{H_2O} + \frac{P_{CO_2}}{K_6} + \sqrt{\frac{P_{H_2}}{K_9}} + \frac{K_2 K_3 K_9 K_4 P_{H_2O}}{P_{H_2}} + \frac{K_3 K_2 \sqrt{K_9} P_{H_2O}}{\sqrt{P_{H_2}}} + \frac{K_1 K_5 P_{CO}\sqrt{P_{H_2}}}{\sqrt{K_9}} + \frac{P_{CO_2}\sqrt{P_{H_2}}}{K_8 K_5 K_7 \sqrt{K_9}}\right)^2}$$

If step 7 (COOH dissociation) is the rate determining step:

$$r_7 = \frac{K_7 K_6 K_1 K_5 K_4 K_3 K_2 \sqrt{K_9}\, P_{CO} P_{H_2O}\, P_{H_2}^{-.5}(1-\beta)}{\left(1 + K_1 P_{CO} + K_2 P_{H_2O} + \frac{P_{CO_2}}{K_6} + \sqrt{\frac{P_{H_2}}{K_9}} + \frac{K_2 K_3 K_9 K_5 K_4 P_{H_2O}}{P_{H_2}} + \frac{K_3 K_2 \sqrt{K_9} P_{H_2O}}{\sqrt{P_{H_2}}} + \frac{K_1 K_5 P_{CO}\sqrt{P_{H_2}}}{\sqrt{K_9}} + K_6 K_1 K_5 K_4 K_3 K_2 \sqrt{K_9\, P_{CO} P_{H_2O}\sqrt{P_{H_2}}}\right)^2}$$

- **Mechanism involving COH & HCOOH**

    (1)   CO + * $\longleftrightarrow$ CO*

    (2) H_2O + * $\longleftrightarrow$ H_2O *

    (3) H_2O* + * $\longleftrightarrow$ OH* + H*

    (4)   CO* + H * $\longleftrightarrow$ COH* + *

    (5)   COH* + OH* $\longleftrightarrow$ HCOOH* + *

    (6)   HCOOH* + 2* $\longleftrightarrow$ CO_2* + 2H *

    (7) CO_2* $\longleftrightarrow$ CO_2 + *

    (8)   2H* $\longleftrightarrow$ H_2* + 2*

If step 4 (OH dissociation) is the rate determining step:

$$r_4 = \frac{K_4 \dfrac{K_1}{\sqrt{K_8}} P_{CO} P_{H_2}^{.5}(1-\beta)}{\left(1 + K_1 P_{CO} + K_2 P_{H_2O} + \frac{P_{CO_2}}{K_7} + \sqrt{\frac{P_{H_2}}{K_8}} + \frac{K_3 K_2 \sqrt{K_8} P_{H_2O}}{\sqrt{P_{H_2}}} + \frac{P_{CO_2} P_{H_2}}{K_8 K_6 K_7} + \frac{P_{CO_2} P_{H_2}\sqrt{P_{H_2}}}{K_2 K_3 K_8 K_5 K_6 \sqrt{K_8}\, P_{H_2O}}\right)^2}$$

35

If step 5 (COH formation) is the rate determining step:

$$r_5 = \frac{K_1 K_5 K_4 K_3 K_2 P_{CO} P_{H_2O}(1-\beta)}{\left(1 + K_1 P_{CO} + K_2 P_{H_2O} + \frac{P_{CO_2}}{K_6} + \sqrt{\frac{P_{H_2}}{K_9}} + \frac{K_3 K_2 \sqrt{K_8} P_{H_2O}}{\sqrt{P_{H_2}}} + \frac{P_{CO} P_{H_2}}{K_6 K_7 K_8} + \frac{K_1 K_4 P_{CO} \sqrt{P_{H_2}}}{\sqrt{K_8}}\right)^2}$$

If step 6 (COOH formation) is the rate determining step:

$$r_6 = \frac{K_6 K_1 K_5 K_4 K_3 K_2 \sqrt{K_8}\, P_{CO} P_{H_2O}(1-\beta)}{\left(1 + K_1 P_{CO} + K_2 P_{H_2O} + \frac{P_{CO_2}}{K_6} + \sqrt{\frac{P_{H_2}}{K_9}} + \frac{K_3 K_2 \sqrt{K_8} P_{H_2O}}{\sqrt{P_{H_2}}} + K_1 K_5 K_4 K_3 K_2 P_{H_2O} P_{CO} + \frac{K_1 K_4 P_{CO} \sqrt{P_{H_2}}}{\sqrt{K_8}}\right)^2}$$

Table 4 summarizes the possible reaction orders obtained according to the reaction mechanisms.

Mechanism	RDS	Reaction Order			
		H_2	CO	CO_2	H_2O
Redox	r_3	0	0	0	1
	r_4	-.5	0	0	1
	r_5	-1	1	0	1
Carboxyl mechanism	r_3	0	0	0	1
	r_4	-.5	1	0	1
	r_5	-.5	1	0	1
Mechanism involving COH	r_4	-.5	0	0	1
	r_5	-.5	1	0	0
	r_6	-.5	1	0	1
	r_7	-.5	1	0	1
Mechanism involving COH & HCOOH	r_4	-.5	1	0	0
	r_5	0	1	0	1
	r_6	0	1	0	1

Table 4.- Theoretical reaction orders for each reaction mechanisms proposed

3.4 Experimental H2 and CO orders

In order to identify the reliance of H_2 and CO partial pressure, and to clarify whether either one or different possible mechanism described in chapter 3.3, defines the reaction order of the WGS reaction mechanism, samples 50 and 75Pd were analyzed by means of different H_2 and CO partial pressures at 450°C in the range of 31.7-5.8 and 23.1 – 5.8 Kpa respectively. All data regarding experimental part is displayed in the **appendix F.**

Along with H_2 and CO, He and CO_2 were used to during each sample testing, the first one as a carrier gas and to balance the volumetric flow to 520 ml/min, CO_2 was used as a reference boundary.

Figures 3.4 and 3.5 display the results obtained during experimental research, both plots denote   positive order; this indicates that can follow the one of the mechanisms previously described. All data collected within these experiments is summarized in **table 5.**
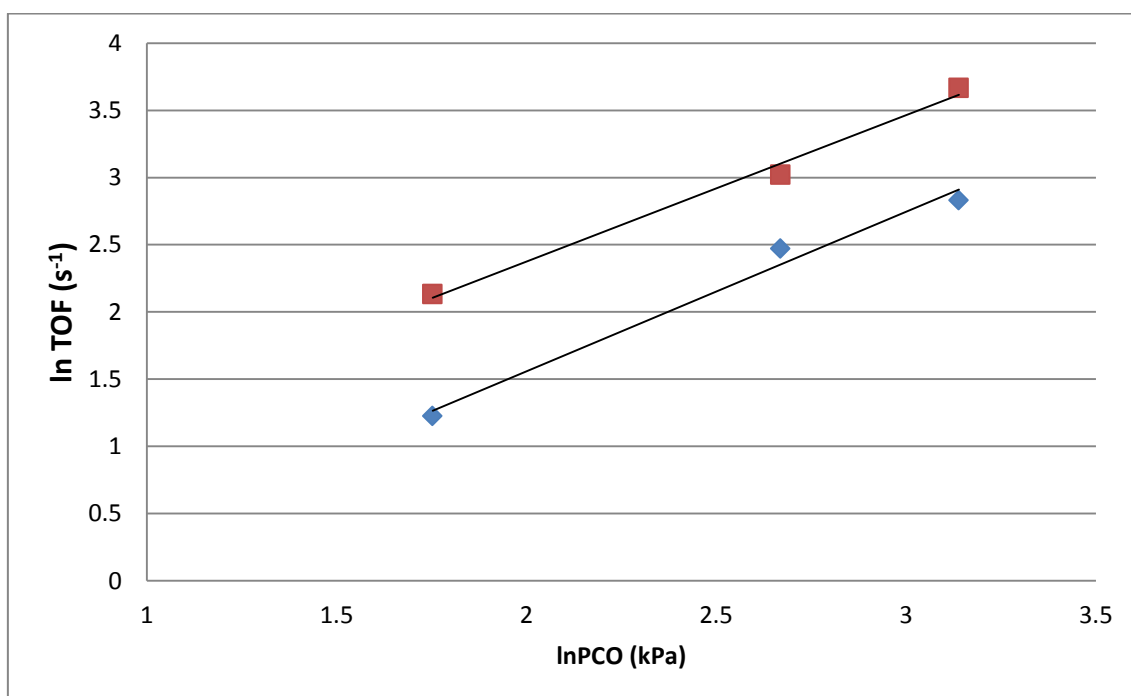
Figure 3.4: dependence of the WGS reaction according to CO partial pressure; from top to bottom sample 3.0Pd/20Ni-20Co HTand 4.5Pd/20Ni-20Co HT (450°C, 1.5 bar, 5.8-23.1 Kpa CO, 57.7 kPa H2O, 26.0 kPa H2, 23.1 kPa CO2, 27.5 – 20.2 kPa He)
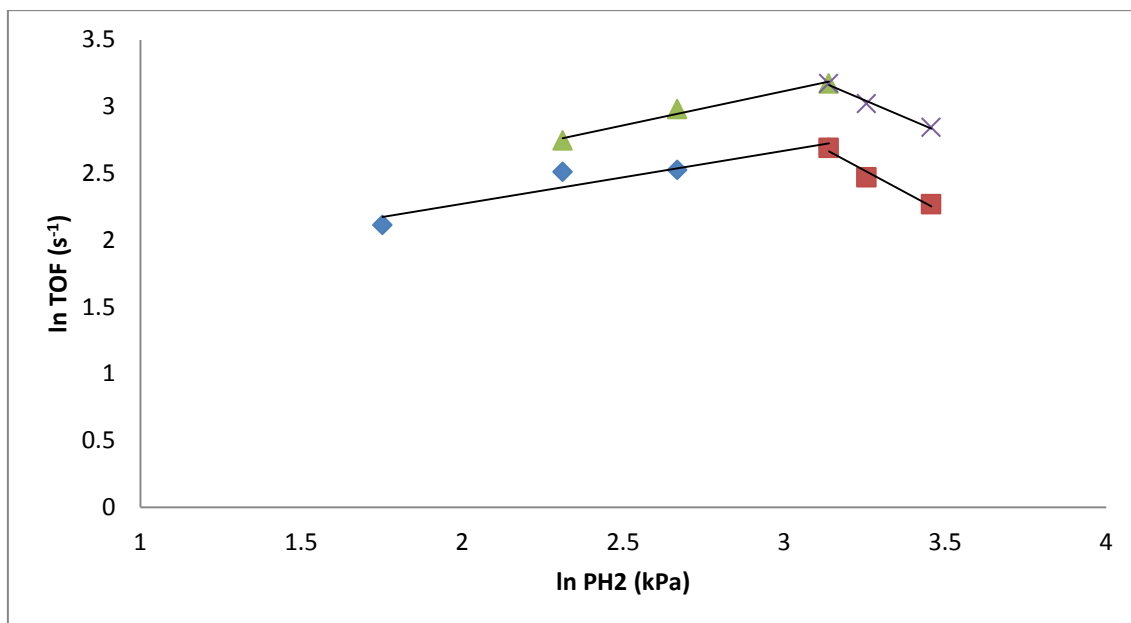
Figure 3.5: dependence of the WGS reaction according to H2 partial pressure; from top to bottom sample 3.0Pd/20Ni-20Co HTand 4.5Pd/20Ni-20Co HT (450°C, 1.5 bar, 14.4 Kpa CO, 57.7 kPa H2O, 5.8 – 31.7 kPa H2, 23.1 kPa CO2, 27.5 – 20.2 kPa He)

3.5 Experimental Activation Order

The activation energy will be defined as the overall energy required to split the strong C-O and H-O-H bonds.
The activation energy is associated with the reaction between adsorbed C, H and O atoms.

For an elementary reaction the temperature dependence of the rate constant is given by the Arrhenius equation.

$$k = Ko^{\left(-\frac{Ea}{RT}\right)}$$

Figure 3.6 outlines the behavior of the reaction rate among $400 - 475°C$ temperature conditions. All data regarding experimental part is displayed in the appendix E2.

38
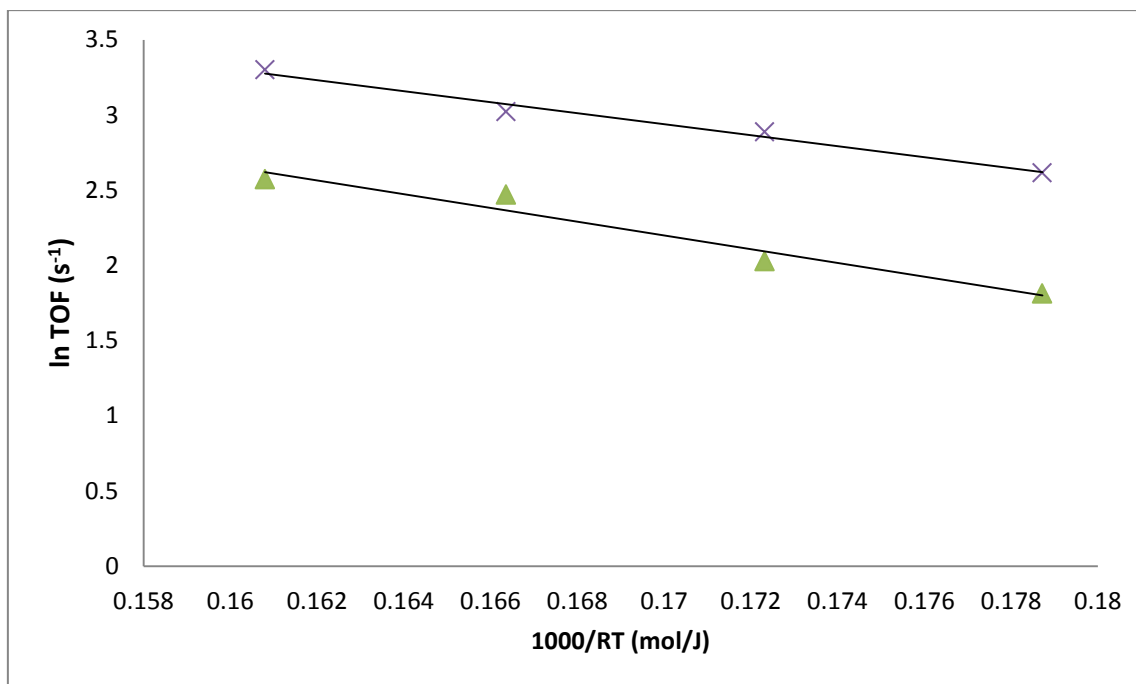
Figure 3.6.- Arrenius plot for HTS reaction; from top to bottom sample 4.5Pd/20Ni-20Co HT and 3.0Pd/20Ni-20Co HT (400- 475°C, 1.5 bar, 14.4 Kpa CO, 57.7 kPa H2O, 26.0 kPa H2, 23.1 kPa CO2, 28.8 kPa He)

Sample Pd %	Kinetic results			
	Ea (kJ/mol)	H2 order		*CO order*
		Low partial pressurre	High partial pressure	
**25 Pd calcined	69.1	.55	-1.07	.91
50 Pd calcined	45.64	.39	-1.28	1.24
75 Pd calcined	36.581	.51	-1.01	1.088

Table 5.- Kinetic data for three metallic catalyst

data collected [50].

Results from the kinetic modeling give the assumption of a first order dependence in the CO rate; however H_2 order has a variation according to the partial pressure. A higher inflow tend to decrease in CO conversion, even it can be seen from tables F2a* and F2b* an escalation in methanation. For a low partial pressure the reaction order will be defined in .5 and -1 for high pressure.

Also the activity of the catalyst follows the Arrhenius like behavior but the increment of Palladium decreases the activation energy on the catalyst which means that Pd enhances the catalyst activity.

3.6 Experimental SEWGS

Experimental WGS was performed into the same conditions for 50 and 75 Pd samples. Inlet composition was carried out under a S/C ratio of 4, with a volumetric flow of 40 ml/min of water and 10 ml/min of CO. In addition He was used as a carrier gas. All reaction cycles were tested at 450°C and a pressure of 150 Kpa.

Figures 3.7 and 3.8 belong both to the sample of 50 Pd and for 75 Pd. At first glance, we can identify a faster deactivation in 75 Pd sample against 50 Pd. **Table 6** summarizes the data concerning the gas yield during SEWGS phase compared with HTS.

According to Unisim simulation the total molar flow of the dry basis components will be of: $.5585 \frac{gmol}{min}$
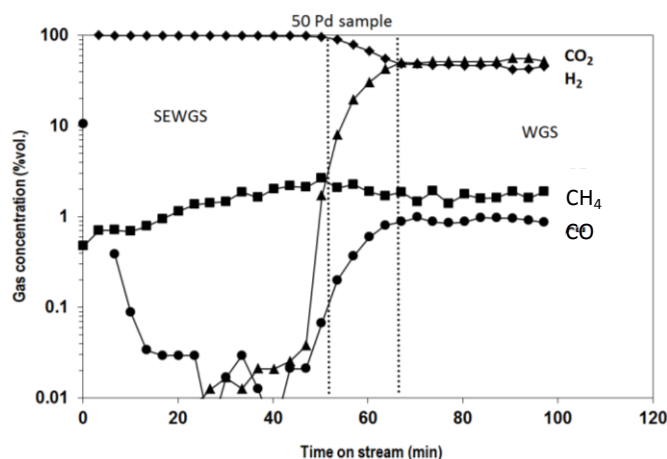
Figure 3.7.- catalyst performance during the first cycle of 50 Pd sample. Gas composition is expressed in dry basis, ◆H$_2$, ▲CO$_2$, ◼ CH$_4$ ● CO. Reaction conditions 450°C, 1.5 atm, volumetric water flow of 40 ml/min and 10 ml/min of CO, catalyst preparation of .4 mg of 3.0Pd/20Ni-20Co HT and 4 gms of dolomite.
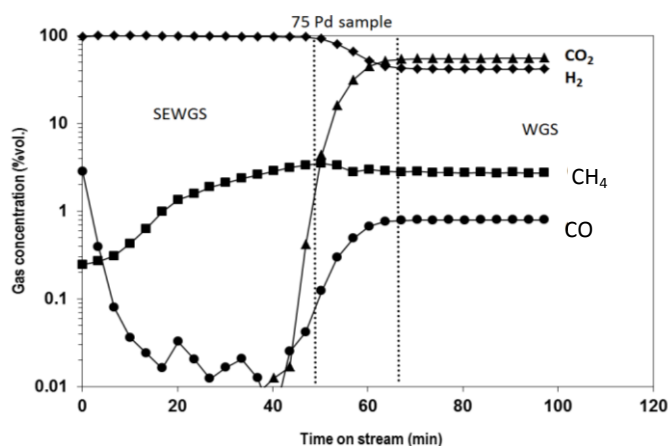
Figure 3.8.- catalyst performance during the first cycle of 75 Pd sample. Gas composition is expressed in dry basis, ◆H$_2$, ▲CO$_2$, ◼ CH$_4$ ● CO. Reaction conditions 450°C, 1.5 atm, volumetric flow of 40 ml/min of water and 10 ml/min of CO, catalyst preparation of .4 mg of 4.5Pd/20Ni-20Co HT and 4 gms of dolomite.

Sample	SEWGS Time on Stream	CO2 inhibed	H2 produced	CH4 inhibed
50Pd	54.5 min	-686.45 gms	31.24gms	-1.34gms
75Pd	51.50 min	-690.91 gms	32.30 gms	-4.72gms

Table 6.- Total mass balance comparition between SEWGS reaction and HTS

According to the average catalyst yield, the comparition between both catalyst slightly favored the 75Pd sample, however according to the tables in appendix G, steady flow of has a higher convertion in 50Pd catalyst.
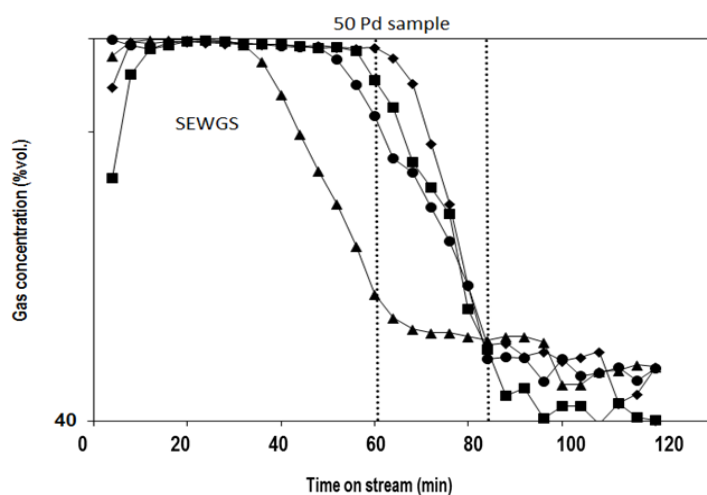
Figure 3.8. - Cyclical hydrogen production for 50 Pd sample. The catalyst has different performance according to the number of cycle, according to the slope,◆first cycle,▲second cycle,■third cycle,●forth cycle. Reaction conditions 450°C, 1.5 atm, volumetric water flow of 40 ml/min and 10 ml/min of CO, catalyst preparation of .4 mg of 3.0Pd/20Ni-20Co HT and 4 gms of dolomite.
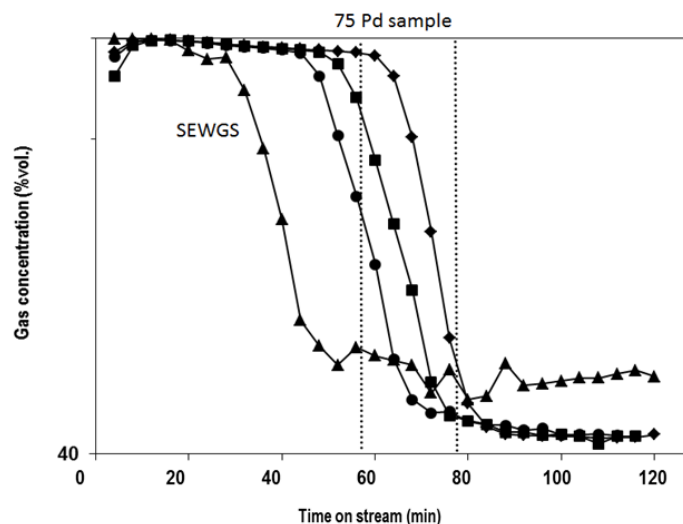
Figure 3.9. - Cyclical hydrogen production for 50 Pd sample. The catalyst has different performance according to the number of cycle, according to the slope,◆first cycle,▲second cycle, ▣third cycle,●forth cycle. Reaction conditions 450°C, 1.5 atm, volumetric water flow of 40 ml/min and 10 ml/min of CO, catalyst preparation of .4 mg of 4.5Pd/20Ni-20Co HT and 4 gms of dolomite.
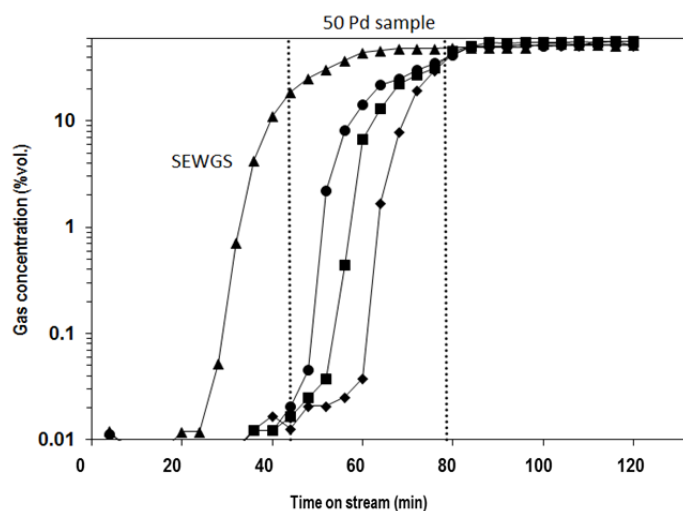
Figure 3.10. - Cyclical CO_2 production for 50 Pd sample. The catalyst has different performance according to the number of cycle, according to the slope, ◆first cycle, ▲second cycle, ▣third cycle, ●forth cycle. Reaction conditions 450°C, 1.5 atm, volumetric water flow of 40 ml/min and 10 ml/min of CO, catalyst preparation of .4 mg of 3.0Pd/20Ni-20Co HT and 4 gms of dolomite.
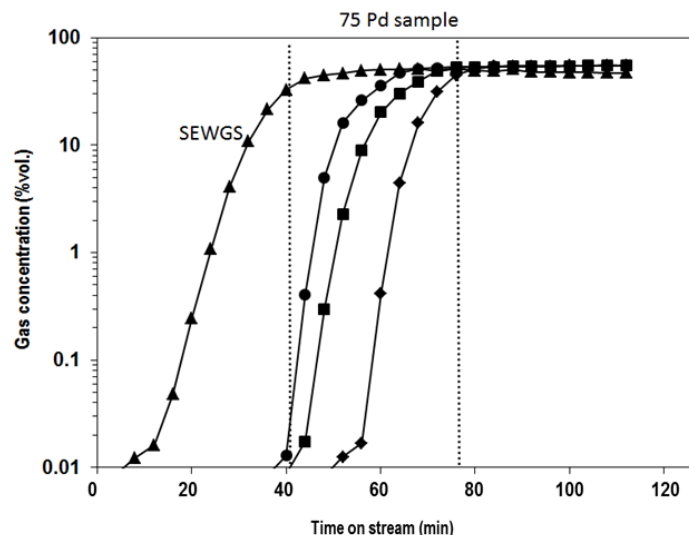
Figure 3.11. - Cyclical CO$_2$ production for 50 Pd sample. The catalyst has different performance according to the number of cycle, according to the slope, ◆first cycle, ▲second cycle, ■third cycle, ●forth cycle. Reaction conditions 450°C, 1.5 atm, volumetric water flow of 40 ml/min and 10 ml/min of CO, catalyst preparation of .4 mg of 4.0Pd/20Ni-20Co HT and 4 gms of dolomite.

As seen in above figures (3.08-3.10) the catalyst is gradually losing its conversion strength. This is caused both by catalyst deactivation and sorbent saturation. Catalyst can deactivate gradually due to sintering, since the desorption of the CO2 is held at high temperatures within a constant flow of 100ml/min of air (exothermic reaction), in the other hand sorbent desaturation must be done at 1000°C (46) for a maximum desorption, otherwise traces of CO2 will kept in the dolomite structure.

Figure 3.12 shows how the SEWGS time on stream decreases by the loss of strength of the catalyst
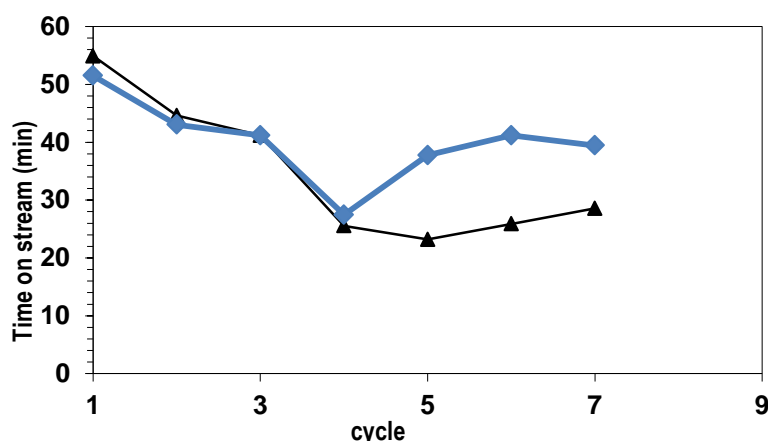
Figure 3.11. – Decrease in timing for the SEWGS reaction. ◆represents sample 50Pd, and ▲sample 75Pd. Reaction conditions 450°C, 1.5 atm, volumetric water flow of 40 ml/min and 10 ml/min of CO, catalyst preparation of .4 mg of catalyst (4.0Pd/20Ni-20Co HT and 4.0Pd/20Ni-20Co HT)and 4 gms of dolomite.

5. Conclusion

From the XRD data we can assume that the catalyst is more like amorphous form, as the peaks aren't so sharp, which indicates that the crystal size is not well developed during the synthesis.

Pd deposition in the catalyst decreases the dispersion and metal surface and thus has the highest crystal size. Calcination facilitates the dispersion of metals in the catalyst.

According to the reaction rates obtained and the reaction mechanism developed step 5 (CO2 formation) from redox mechanism seems to be a profitable rate equation at high hydrogen orders. But this reaction rate is no accurate at low hydrogen partial pressure.

Among 50 and 75 samples, 50 present the best conversion, but not the best selectivity. Kinetic experiments demonstrate that methanation decreases according to the increment of Pd in the catalyst.

SEWGS experiments demonstrate a high increment compared to both experimental steady state and simulation equilibrium conversion. From both catalysts, 75 and 50 Pd, 50 Pd shows a higher yield during SEWGS and HTS reactions.

Abbreviations & Symbols

β	----	Equilibrium factor
D	----	Dispersion
Ø	----	Diamter
Ea	----	Activation energy
GC	----	Gas chromatography
HL	----	Hydrolytic liquefaction
HT	----	Hydrotalcite
HTS	----	High temperature water gas shift
LTS	----	Low temperature water gas shift
R	----	Universal Gas constant
S/C	----	Steam carbon ratio
SEM	----	Scanning electron microscope
SESR	----	Sorption enhance water gas shift
SEWGS	----	Sorption enhance steam reforming
SR	----	Steam reforming
Vabs	----	Volume adsorbed at the surface
WGS	----	Water Gas shift
XRD		X-ray Diffraction

REFERENCES

1) R. H. Hirsch, R. Bezdek, R. Wendling, "Peaking of world oil production: Impacts, mitigation, and risk managemenf. *US National Energy Technology Laboratory Report,* Febr. 2005, 91 pp.; http:/ www.oilcrisis.comfUSfNETLfOilPeaking.pdf

2) L. He, H. Berntsen and D. Chen, J. Phys. Chem. A, 2009, 114, 3834–3844.

3) J. Fermoso, L. He and D. Chen. Sorption enhanced steam reforming (SESR): a direct route towards efficient hydrogen production from biomass-derived compounds. Society of Chemical Industry. Feb 2012. www.wileyonlinelibrary.com/jctb

4) G. Wu, C. Zhang, S. Li, Z. Huang, S. Yan, S. Wang, X. Maand, J. Gong, "Sorption enhanced steam reforming of ethanol on Ni–CaO–Al2O3 multifunctional catalysts derived from hydrotalcite-like compounds". Energy& Environmental Science. October 2012 pp 8765-9136

5) J. Fermoso, F. Rubiera, D. Chen "Sorption enhanced catalytic steam gasification process: a direct route from lignocellulosic biomass to high purity hydrogen". Energy& Environmental Science. 2012 pp 6358-6367

6) B. Dou, G. L. Rickett, V. Dupont, P. T. Williams, H. Chen, Y. Ding, M.Ghadiri "Steam reforming of crude glycerol with in situ CO2 sorption" Bioresource Technology 101 (2010) 2436–2442

7) Froment G. F. and Bischoff K. B. Chemical Reactor Analysis and Design; (1990) 2nd ed. pp. 462-591

8) C. E. Daza, S. Moreno "Ce – Promoted Catalyst From Hydrotalcites For $C0_2$ Reforming Of Methane: Calcination Temperature Effect" Quim. Nova, Vol. 35, No. 7, 1325-1328, 2012

9) K. Kaneda, K. Yamaguchi, K. Mori, T. Mizugaki, K. Ebitani "Catalyst design of hydrotalcite compounds for efficient oxidations" Catalysis Surveys *from Japan* 4 (2000) 31–38

10) H.Th.J. Reijers, S.E.A. Valster-Schiermeier, P.D. Cobden and R.W. van den Brink "Hydrotalcite as CO_2 sorbent for sorptionenhanced steam reforming of methane" *Ind. Eng. Chem. Res.*, 2006, 45 (8), pp 2522–2530

11) E. Ochoa-Fernandeza, C. Lacalle-Vila, K. Christensena,c, J.C. Walmsleyb, M. Rønning, A. Holmen, and D. Chen "Ni catalysts for sorption enhanced steam methane reforming"

12) E. S. Wangen, A. Osatiashtiani, E. A. Blekkan "Reforming of Syngas from Biomass Gasification: Deactivation by Tar and Potassium Species" Top Catal (2011) 54:960–966

13) L. He, H. Berntsen, E. OchoaFernandez, J. C. Walmsley, E. A. Blekkan, D. Chen "Co–Ni Catalysts Derived from Hydrotalcite-Like Materials for Hydrogen Production by Ethanol Steam Reforming" Top Catal (2009) 52:206–217

14) X. Hu, G. Lu "Investigation of the steam reforming of a series of model compounds derived from bio-oil for hydrogen production" Applied Catalysis B: Environmental 88 (2009) 376–385

15) J. Anderson, M. Garcia "Supported Metals in Catalysis" Catalytic Science Series Vol 5 2005 pag 123-130, 229-273

16) Chorkendorff, J.W. Niemantsverdriet "Concepts of Modern Catalysis and Kinetics" 2003 WILEY-VCH Verlag GmbH & Co. KGaA, Weinheim ISBN: 3-527-30574-2

17) D. Chen, L. He "Towards an Efficient Hydrogen Production from Biomass: A Review of Processes and Materials" ChemCatChem 2011, 3, 490 – 511

18) The Quantum Coherence Lab at the Department of Physics, University of Basel. http://zumbuhllab.unibas.ch/pdf/talks/080425_Tobias_BET.pdf

19) Moe, J.M., Design of water-gas shift reactors. Chem. Eng. Prog. 1962, 58 (3), 33-36.

20) Kamm, B.; Gruber, P.R.; Kamm, M. (Biorefineries -- Industrial Processes and Products", Wiley-VCH) pag 116, 121

21) Christina Hornell "thermochemical and catalytic Upgrading in a fuel context: peat, biomass and Alkenes" Royal Institute of Technology Engineering and Technology, Chemical Technology, Stockholm 2001

22) Umakanta Jena, K.C Das " Comparative evaluation of thermochemical liquefaction and Pyrolysis for Bio-Oil Production from microalgae" Energy&Fuel articl, ACS publications, American Chemistry Society 2011

23) Wisconsin biorefining development initiative "Biorefining Process- Thermochemical Liquefaction" www.wisbiorefine.org

24) Maria P. Aznar, Miguel A. Caballero, Jose Corella, Gregorio Molina and José M. Toledo "Hydrogen Production by Biomass Gasification with Steam-O2 Mixtures Followed by a Catalytic Steam Reformer and a CO-Shift System" Energy & Fuels 2006, 20, 1305-1309

25) P. Spath, A. Aden, T. Eggeman, M. Ringer, B. Wallace, and J. Jechura "Biomass to Hydrogen Production Detailed Design and Economics Utilizing the Battelle Columbus Laboratory Indirectly-Heated Gasifier" National Renewable Energy Laboratory Technical report NREL/TP-510-37408 May 2005

26) Figure 1B http://chemistry.about.com/od/factsstructures/ig/Chemical-Structures---G/Glucose.htm

27) Meyers R.A. (2004). Handbook of petroleum refining processes. 3rd ed., part 6.25

28) Zhang, R., Cummer, K., Suby, A., and Brown, R. C., Biomass-derived hydrogen from an air-blown gasifier," Fuel Processing Technology 86, 861-874, 2005

29) George W. Huber, Sara Iborra, and Avelino Corma* "Synthesis of Transportation Fuels from Biomass: Chemistry, Catalysts, and Engineering" Instituto de Tecnologıa Quımicia, UPV-CSIC, Chem. Rev. 2006, 106, 4044☐4098

30) L. Lloyd, D.E. Ridler, M.V. Twigg, in: M.V. Twigg (Ed.), Catalysis Handbook, Wolfe Scientific Books, London 1996. p. 339.

31) Genira Carneiro de Araújo, Maria do Carmo Rangel "An environmental friendly dopant for the high-temperature shift catalysts" Catalysis Today 62 (2000) 201–207

32) D. Mendes, A. Mendes, L. M. Madeira, A. Iulianelli, J. M. Sous and A. Basile "The water-gas shift reaction: from conventional catalytic systems to Pd-based membrane reactors – a review" Asia-Pac. J. Chem. Eng. 2010; 5: 111–137

33) M.- San Shwe Hla,G. J. Duffy, L. D. Morpeth, A. Cousins,D. G. Roberts, J. H. Edwards and D. Park "Catalysts for water–gas shift processing of coal-derived syngases" Asia-Pac. J. Chem. Eng. 2010; 5: 585–592

34) Sung Ho Kima, Suk-Woo Namb, Tae-Hoon Limb, Ho-In Lee "Effect of pretreatment on the activity of Ni catalyst for CO removal reaction by water–gas shift and methanation" Applied Catalysis B: Environmental 81 (2008) 97–104

35) Masatoshi Nagai, Amin Md. Zahidul, Yutaka Kunisaki, Yusuke Aoki "Water–gas shift reactions on potassium- and zirconium-promoted cobalt molybdenum carbide catalysts" Applied Catalysis A: General 383 (2010) 58–65

36) Richard g. Copperthwaite", Frank m. Gottschalk" and Tarnya Sangiorgio "Cobalt Chromium Oxide: A Novel Sulphur Tolerant Water-Gas Shift Catalyst" Applied Catalysis, 63 (1990) Lll-L16

37) Carlos Enrique Daza, Sonia Moreno and Rafael Molina* "Ce – PROMOTED CATALYST FROM HYDROTALCITES FOR CO2 REFORMING OF METHANE: CALCINATION TEMPERATURE EFFECT" Quim. Nova, Vol. 35, No. 7, 1325-1328, 2012

38) Alak Bhattacharyya, Victor W. Chang, Daniel J. Schumacher "CO reforming of methane to syngas I: evaluation of hydrotalcite clay-derived catalysts" Applied Clay Science 13 1998 317–328

39) W. Ruettinger, J. Lampert, O. Korotikkh and R.J Farrauto «Non-Pyrophoric Water-Gas Shift Cataysts for Hydrogen Generation in Fuel Cell Applications" Abstr AP AM Chemo S 221: 11-Fuel Part 1

40) D.C Grenoble and M.M Estadt " The chemistry and catalysis of the water gas shift reaction" journal of catalysis 67, 90-102 (1981)

41) S. Hilaire,, X. Wang, , T. Luo, R.J. Gorte, J. Wagner "A comparative study of water-gas-shift reaction over ceria supported metallic catalysts" Applied Catalysis A: General 215 (2001) 271–278

42) GG.- Johnsen K and Grace JR, High-temperature attrition of sorbents and a catalyst for sorption-enhanced steam methane reforming in a fluidized bed environment. Powder Technol 173:200–202 (2007).

43) C. V. OVESEN, P. STOLTZE, J. K. N•RSKOV AND C. T. CAMPBELL "A Kinetic Model of the Water Gas Shift Reaction" JOURNAL OF CATALYSIS 134, 445-468 (1992)

44) Wheeler C, A. Jhalani, E.J. Klein, S. Tummala, and L.D. Schmidt, "The water–gas-shift reaction at short contact times" Journal of Catalysis, 223, 2004,191–199

45) Phatak A A, N. Koryabkina, S. Rai, J.L. Ratts, W. Ruettinger, R.J. Farrauto, G.E. Blau, W.N. Delgass and F.H. Ribeiro, "Kinetics of the water–gas shift reaction on Pt catalysts supported on alumina and ceria", Catalysis Today,123, 2007, 224–234

46) George L. Kan, Arthur M. Squires, Robert A. Graff "High Pressure TGA Studies on the Cyclic Use of Half-Calcined Dolomite to Remove Hydrogen Sulfide" The clean Fuels Institute Department of Chemical Engineering The city College of New York New York, N.Y. 10031

47) Kyung-Ran Hwang, Chun-Boo Lee, Jong-Soo Park "Advanced nickel metal catalyst for water–gas shift reaction" Journal of Power Sources 196 (2011) 1349–1352

48) Bent Sørensen "Hydrogen and fuel cells" Elsevier Academic Press, Oxord OX5 1GB UK, pag 99

49) Li He and De Chen "Single-Stage Production of Highly Concentrated Hydrogen from Biomass-Derived Syngas" DOI: 10.1002/cssc.201000167

50) Tayyaba Noor "Sorption Enhance High Temperature Water Gas Shift Reaction; Materials and Catalyst" Doctoral thesis at NTNU 2013:181

APPENDIX A

The catalytic base composition has been calculated under previous works [13]. Table Ax belongs to the Mass weight per component regarding the preparation of 100mg.

Sample Pd %	Catalytic base composition					
	Cation solution (mg)				Anion Solution (mg)	
	$Mg(NO_3)_2.H_2O$	$Co(NO_3)2.6H_2O$	$Ni(NO_3)_2.6H_2O$	$Al(NO_3)_3.9H_2O$	Na_2CO_3	NaOH
0	31,972	14,567	14,614	28,135	5,962	23,998
25.00	31,972	14,567	14,614	28,135	5,962	23,998
50.00	31,972	14,567	14,614	28,135	5,962	23,998
75.00	31,972	14,567	14,614	28,135	5,962	23,998

Table AX. - Pd/Ni-CO HT Catalyst preparation at 100 mg base

Appendix B

Considering previous research projects [13] it can be defined that the total dispersion for a 20Co-20Ni HT catalyst corresponds to 8.7%.

According to this, we can make the following analogy.

$$.087\,\frac{g(Ni+Co\ Surface)}{g(Ni+Co)total}\ X\ \frac{40\ g\ (Ni+Co)total}{100g\ Catalyst}=.0348\,\frac{g(Ni+Co\ Surface)}{gCatalyst}$$

$$.0348\,\frac{g(Ni+Co\ Surface)}{gCatalyst}X\ \frac{1\ mol\ (Ni+Co)}{58.8g(Ni+Co\ Surface)}=5.9184*10^{-4}\,\frac{mol\ Pd\ (Max)}{gCatalyst}$$

Ni   Molar Weight= 58.7 u
Co   Molar Weight= 58.9 u
Pd   Molar Weight= 106.4 u

$$\dot{M}(Ni+Co)=\frac{58,7+58,9}{2}=58,8\ g/mol$$

If we consider a 100% of reaction between Ni and Co molecules with Pd in a ratio of 1 we will get:

$$\frac{Pd}{Ni}=1$$
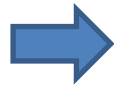
$$5.9184*10-4\,\frac{mol\ Pd\ (Max)}{gCatalyst}\ X\ 106,4\,\frac{g}{mol}$$

$$\frac{Pd}{Co}=1$$

At a 100% Pd sample the mas of Pd will be:

$$.062979\ \frac{g\ Pd}{g\ catallyst}$$

In order to prepare the Pd dissolution:

$Pd(NO_3)_2 \cdot 2H_2O$ **Molar Weight= 266,43 u**

The ratio of Pd content will be.

$$.40\ \frac{g\ Pd}{g\ Pd(NO3)2\cdot2H2O}$$

Considering the required at a 100%

$$.062979 \ \frac{\textbf{g Pd}}{\textbf{g catallyst}} \ \textbf{X} \ \textbf{40}^{-1} \ \frac{\textbf{g Pd(NO3)2·2H2O}}{\textbf{g Pd}} \ \textbf{X 100}$$

For the 100% composition we must dissolve

$$.157 \ \frac{\textbf{g Pd(NO3)2·2H2O}}{\textbf{g catallyst}}$$

Same procedure is repeated, but considering a lower percentage of Pd molecules interacting with the Ni and Co molecules

C

Appendix C

Compound	Formula	M.W	State	Purity	Supplier
Magnesium nitrate Hexahydrate	$Mg(NO3)2 \cdot H2O$	**256.41**	**S**	**≥ 99.99**	**Sigma Aldrich**
Cobalt(II) nitrate Hexahydrate	$Co(NO3)2 \cdot 6H2O$	**291.04**	**S**	**≥ 99.99**	**Merck**
Nickel (II) nitrate Hexahydrate	$Ni(NO3)2 \cdot 6H2O$	**290.81**	**S**	**≥ 99.99**	**Fluka**
Aluminum nitrate Nonahydrate	$Al(NO3)3 \cdot 9H2O$	**375.13**	**S**	**≥ 99.99**	**Sigma Aldrich**
Sodium Carbonate	Na_2CO_3	**105.99**	**S**	**≥ 99.99**	**VWR**
Sodium Hydroxide	$NaOH$	**40**	**S**	**≥ 99.99**	**Merck**
Palladium(II) nitrate Dihydrate	$Pd(NO_3)_2 \cdot 2H_2O$	**266.43**	**S**	**≥ 99.99**	**Sigma Aldrich**
Nitrogen	N_2	**28**	**G**	**≥ 99.999**	**Yara Praxair**
Hydrogen	H_2	**2**	**G**	**≥ 99.999**	**Yara Praxair**

Table C.1 – Chemical List

Appendix D

As an example for dispersion calculations we will use the isotherms obtained from chemisorption during the characterization of samples 0 and 50 (calcined one).
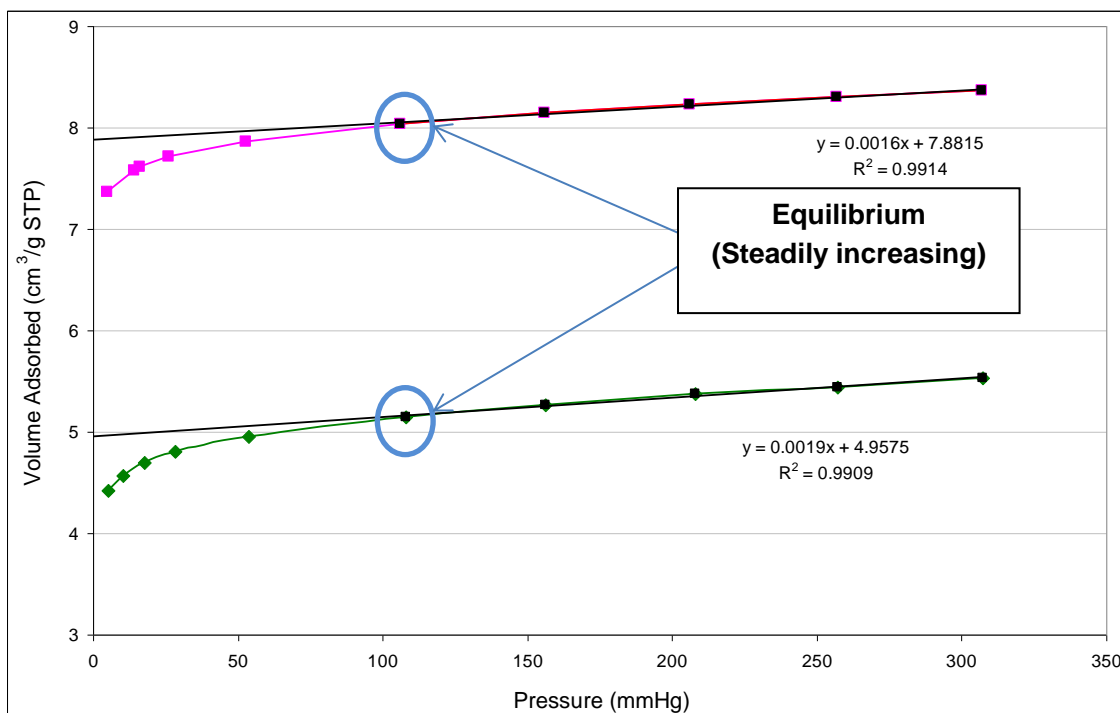
Figure D1.- Adsorbtion isotherms for Pd(50%)/ Ni-Co HT and single Ni-Co HT

As mention in chapter 3.2, V_{abs} must be calculated at total vacuum conditions. Table D1 display the values of V_{abs} obtained extrapolating the data from the steadily behavior.

Sample	V_{abs} (mass base) @ 0 mmHg
0	7,88
50	4.95

Table D1 – H2 chemisorbet @ 0 mmHg

V_{abs} obtained must be expressed in molar base, for this purpose it is suitable to make the following analogy.

$$Vads\left(\frac{mol}{gcat}\right) = Vads\left(\frac{cm^3}{gcat}\right) x \frac{P}{RT}$$

Were R is the universal gas constant, P and T means pressure and temperature at standard conditions.

Table D2 presents the values obtained after substitution:

$$Vads\left(\frac{mol}{gcat}\right) = 7.88 \left(\frac{\frac{cm^3}{gcat}}{\frac{10^3 cm^3}{L}}\right) x \frac{1\ atm}{.082057 \left(\frac{atm*L}{mol*K}\right) x\ 273.15K}$$ **Sample 0**

$$Vads\left(\frac{mol}{gcat}\right) = 4.93 \left(\frac{\frac{cm^3}{gcat}}{\frac{10^3 cm^3}{L}}\right) x \frac{1\ atm}{.082057 \left(\frac{atm*L}{mol*K}\right) x\ 273.15K}$$ **Sample 50**

Sample	V_{ads} (molar base) @ 0 mmHg
0	0.000351
50	0.000220

Table D2 – H2 chemisorbet @ 0 mmHg

With the V_{ads} in molar base, it is possible to use the formula for dispersion (this formula has been already explained in chapter 1.3.3).

Recalling from appendix B

Ni   Molar Weight= 58.7 u
Co   Molar Weight= 58.9 u
Pd   Molar Weight= 106.4 u

$$\dot{M}_{metals} = \frac{\sum_{i=1}^{n} X_i}{n}$$

Substituting

$$D(\%) = \frac{.000351 \left(\frac{mol}{gcat}\right) x\ 58.8215 \left(\frac{g}{mol}\right)}{\frac{1}{2} \frac{Molec\ H2}{Molec\ (Ni,Co)} x\ .4 \frac{g\ Co + Ni}{gcat}} x\ 100$$ **Sample 0**

$$D(\%) = \frac{.00022\left(\frac{mol}{gcat}\right) \times 62.34\left(\frac{g}{mol}\right)}{\frac{1}{2}\frac{Molec\ H2}{Molec\ (Ni,Co,Pd)} \times .418\ \frac{g\ Co + Ni + Pd}{gcat}} \times 100$$

Sample 50

Sample	D (%)
0	10.323
50	6.65

Average diameter of the sample can be calculated in the mean of partial diameter of particles.

d(Pd-Co-Ni)(nm)= $\left(\frac{116}{D\%} \times \frac{Pd(\%)}{100}\right) + \left(\frac{96}{D\%} \times \frac{Co(\%)}{100}\right) + \left(\frac{101}{D\%} \times \frac{Ni(\%)}{100}\right)$

Sample 0

d(Co-Ni)(nm)= $\left(\frac{96}{D\%} \times \frac{Co(\%)}{100}\right) + \left(\frac{101}{D\%} \times \frac{Ni(\%)}{100}\right)$

Sample 50

Sample	d (nm)
0	9.5
50	15.4

Appendix E

Figure E1 describes Unisims schematic representation of the reactor and splitter unit used to simulate de experimental conditions during SEWGS tryouts.

12		
Temperature	450.0	C
Pressure	1.500	bar
Molar Flow	2.501	gmole/min
Master Comp Volume Flow (H2O)	0.0024	m3/h
Master Comp Volume Flow (CO)	0.0006	m3/h

24		
Temperature	50.00	C
Pressure	1.500	bar
Molar Flow	0.5585	gmole/min
Mass Flow	0.7756	kg/h
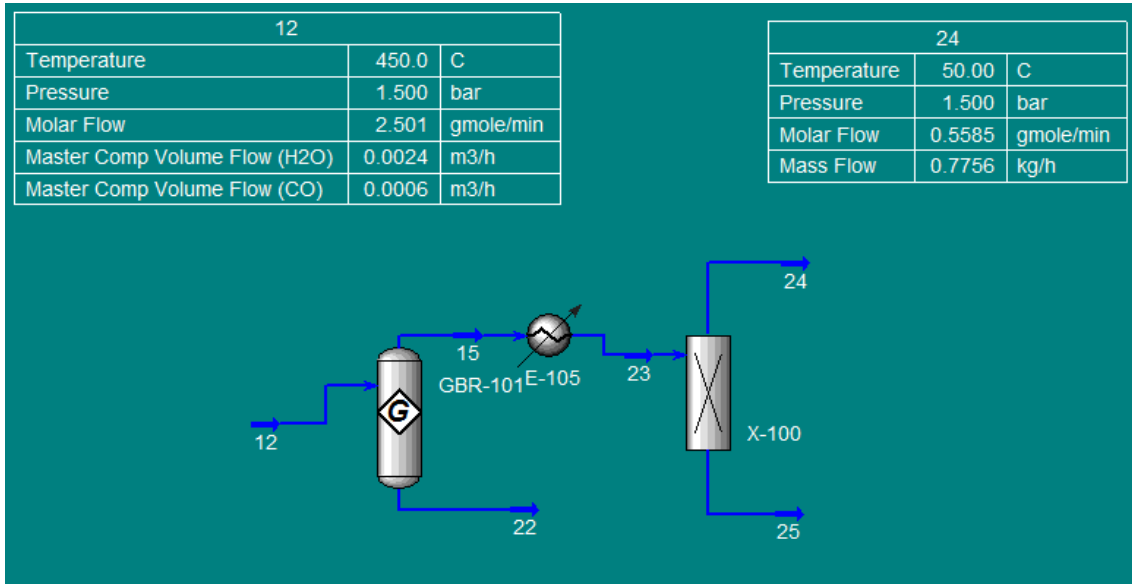
Figure E1.- schemetic model of the equilibrium methanation and WGS reactions at 450°C, 1.5 atm, volumetric water flow of 40 ml/min and 10 ml/min of CO. the sppliter unit is used to calculate a dry yield.

The following data sheets belong to the mass balance and main inlet conditions in each stream.

Case Name:	C:\Users\Christian\Desktop\wgs1.usc
Unit Set:	NewUser
Date/Time:	Friday Jun 28 2013, 18:13:35

Material Stream: 12

Fluid Package:	Basis-1
Property Package:	Peng-Robinson

CONDITIONS

		Overall	Vapour Phase			
Vapour / Phase Fraction		1.0000	1.0000			
Temperature:	(C)	450.0 *	450.0			
Pressure:	(bar)	1.500 *	1.500			
Molar Flow	(gmole/min)	2.501	2.501			
Mass Flow	(g/min)	47.91	47.91			
Std Ideal Liq Vol Flow	(mL/min)	50.00 *	50.00			
Molar Enthalpy	(kJ/kgmole)	-2.120e+005	-2.120e+005			
Molar Entropy	(kJ/kgmole-C)	202.3	202.3			
Heat Flow	(kJ/h)	-3.182e+004	-3.182e+004			
Liq Vol Flow @Std Cond	(mL/min)	50.94	50.94			

COMPOSITION

Overall Phase

Vapour Fraction 1.0000

COMPONENTS	MOLAR FLOW (kgmole/h)	MOLE FRACTION	MASS FLOW (kg/h)	MASS FRACTION	LIQUID VOLUME FLOW (m3/h)	LIQUID VOLUME FRACTION
Methane	0.0000 *	0.0000 *	0.0000 *	0.0000 *	0.0000 *	0.0000 *
Ethane	0.0000 *	0.0000 *	0.0000 *	0.0000 *	0.0000 *	0.0000 *
Propane	0.0000 *	0.0000 *	0.0000 *	0.0000 *	0.0000 *	0.0000 *
i-Butane	0.0000 *	0.0000 *	0.0000 *	0.0000 *	0.0000 *	0.0000 *
i-Pentane	0.0000 *	0.0000 *	0.0000 *	0.0000 *	0.0000 *	0.0000 *
Hydrogen	0.0000 *	0.0000 *	0.0000 *	0.0000 *	0.0000 *	0.0000 *
CO2	0.0000 *	0.0000 *	0.0000 *	0.0000 *	0.0000 *	0.0000 *
CO	0.0171 *	0.1141 *	0.4796 *	0.1668 *	0.0006 *	0.2000 *
H2O	0.1330 *	0.8859 *	2.3952 *	0.8332 *	0.0024 *	0.8000 *
H2S	0.0000 *	0.0000 *	0.0000 *	0.0000 *	0.0000 *	0.0000 *
Air	0.0000 *	0.0000 *	0.0000 *	0.0000 *	0.0000 *	0.0000 *
Oxygen	0.0000 *	0.0000 *	0.0000 *	0.0000 *	0.0000 *	0.0000 *
Nitrogen	0.0000 *	0.0000 *	0.0000 *	0.0000 *	0.0000 *	0.0000 *
Total	0.1501	1.0000	2.8748	1.0000	0.0030	1.0000

Vapour Phase

Phase Fraction 1.000

COMPONENTS	MOLAR FLOW (kgmole/h)	MOLE FRACTION	MASS FLOW (kg/h)	MASS FRACTION	LIQUID VOLUME FLOW (m3/h)	LIQUID VOLUME FRACTION
Methane	0.0000	0.0000	0.0000	0.0000	0.0000	0.0000
Ethane	0.0000	0.0000	0.0000	0.0000	0.0000	0.0000
Propane	0.0000	0.0000	0.0000	0.0000	0.0000	0.0000
i-Butane	0.0000	0.0000	0.0000	0.0000	0.0000	0.0000
i-Pentane	0.0000	0.0000	0.0000	0.0000	0.0000	0.0000
Hydrogen	0.0000	0.0000	0.0000	0.0000	0.0000	0.0000
CO2	0.0000	0.0000	0.0000	0.0000	0.0000	0.0000
CO	0.0171	0.1141	0.4796	0.1668	0.0006	0.2000
H2O	0.1330	0.8859	2.3952	0.8332	0.0024	0.8000
H2S	0.0000	0.0000	0.0000	0.0000	0.0000	0.0000
Air	0.0000	0.0000	0.0000	0.0000	0.0000	0.0000
Oxygen	0.0000	0.0000	0.0000	0.0000	0.0000	0.0000
Nitrogen	0.0000	0.0000	0.0000	0.0000	0.0000	0.0000
Total	0.1501	1.0000	2.8748	1.0000	0.0030	1.0000

Material Stream: 15

Fluid Package:	Basis-1
Property Package:	Peng-Robinson

CONDITIONS

		Overall	Vapour Phase	Liquid Phase	Aqueous Phase	
Vapour / Phase Fraction		1.0000	1.0000	0.0000	0.0000	
Temperature:	(C)	558.0	558.0	558.0	558.0	
Pressure:	(bar)	1.500	1.500	1.500	1.500	

Honeywell
Company Name Not Available
Calgary, Alberta
CANADA

Material Stream: 15 (continued)

Fluid Package:	Basis-1
Property Package:	Peng-Robinson

CONDITIONS

		Overall	Vapour Phase	Liquid Phase	Aqueous Phase
Molar Flow	(gmole/min)	2.501	2.501	0.0000	0.0000
Mass Flow	(g/min)	47.91	47.91	0.0000	0.0000
Std Ideal Liq Vol Flow	(mL/min)	57.96	57.96	0.0000	0.0000
Molar Enthalpy	(kJ/kgmole)	-2.121e+005	-2.121e+005	-2.121e+005	-2.121e+005
Molar Entropy	(kJ/kgmole-C)	207.3	207.3	207.3	207.3
Heat Flow	(kJ/h)	-3.182e+004	-3.182e+004	0.0000	0.0000
Liq Vol Flow @Std Cond	(mL/min)	54.92	54.93	0.0000	0.0000

COMPOSITION

Overall Phase   Vapour Fraction   1.0000

COMPONENTS	MOLAR FLOW (kgmole/h)	MOLE FRACTION	MASS FLOW (kg/h)	MASS FRACTION	LIQUID VOLUME FLOW (m3/h)	LIQUID VOLUME FRACTION
Methane	0.0000	0.0001	0.0003	0.0001	0.0000	0.0003
Ethane	0.0000	0.0000	0.0000	0.0000	0.0000	0.0000
Propane	0.0000	0.0000	0.0000	0.0000	0.0000	0.0000
i-Butane	0.0000	0.0000	0.0000	0.0000	0.0000	0.0000
i-Pentane	0.0000	0.0000	0.0000	0.0000	0.0000	0.0000
Hydrogen	0.0164	0.1092	0.0330	0.0115	0.0005	0.1360
CO2	0.0165	0.1096	0.7240	0.2518	0.0009	0.2523
CO	0.0007	0.0043	0.0182	0.0063	0.0000	0.0066
H2O	0.1165	0.7766	2.0992	0.7302	0.0021	0.6049
H2S	0.0000	0.0000	0.0000	0.0000	0.0000	0.0000
Air	0.0000	0.0000	0.0000	0.0000	0.0000	0.0000
Oxygen	0.0000	0.0000	0.0000	0.0000	0.0000	0.0000
Nitrogen	0.0000	0.0000	0.0000	0.0000	0.0000	0.0000
Total	0.1500	1.0000	2.8748	1.0000	0.0035	1.0000

Vapour Phase   Phase Fraction   1.000

COMPONENTS	MOLAR FLOW (kgmole/h)	MOLE FRACTION	MASS FLOW (kg/h)	MASS FRACTION	LIQUID VOLUME FLOW (m3/h)	LIQUID VOLUME FRACTION
Methane	0.0000	0.0001	0.0003	0.0001	0.0000	0.0003
Ethane	0.0000	0.0000	0.0000	0.0000	0.0000	0.0000
Propane	0.0000	0.0000	0.0000	0.0000	0.0000	0.0000
i-Butane	0.0000	0.0000	0.0000	0.0000	0.0000	0.0000
i-Pentane	0.0000	0.0000	0.0000	0.0000	0.0000	0.0000
Hydrogen	0.0164	0.1092	0.0330	0.0115	0.0005	0.1360
CO2	0.0165	0.1096	0.7240	0.2518	0.0009	0.2523
CO	0.0007	0.0043	0.0182	0.0063	0.0000	0.0066
H2O	0.1165	0.7766	2.0992	0.7302	0.0021	0.6049
H2S	0.0000	0.0000	0.0000	0.0000	0.0000	0.0000
Air	0.0000	0.0000	0.0000	0.0000	0.0000	0.0000
Oxygen	0.0000	0.0000	0.0000	0.0000	0.0000	0.0000
Nitrogen	0.0000	0.0000	0.0000	0.0000	0.0000	0.0000
Total	0.1500	1.0000	2.8748	1.0000	0.0035	1.0000

Liquid Phase   Phase Fraction   0.0000

COMPONENTS	MOLAR FLOW (kgmole/h)	MOLE FRACTION	MASS FLOW (kg/h)	MASS FRACTION	LIQUID VOLUME FLOW (m3/h)	LIQUID VOLUME FRACTION
Methane	0.0000	0.0001	0.0000	0.0001	0.0000	0.0003
Ethane	0.0000	0.0000	0.0000	0.0000	0.0000	0.0000
Propane	0.0000	0.0000	0.0000	0.0000	0.0000	0.0000
i-Butane	0.0000	0.0000	0.0000	0.0000	0.0000	0.0000
i-Pentane	0.0000	0.0000	0.0000	0.0000	0.0000	0.0000
Hydrogen	0.0000	0.1092	0.0000	0.0115	0.0000	0.1360
CO2	0.0000	0.1096	0.0000	0.2518	0.0000	0.2523
CO	0.0000	0.0043	0.0000	0.0063	0.0000	0.0066

J

Honeywell
Company Name Not Available
Calgary, Alberta
CANADA

Case Name:	C:\Users\Christian\Desktop\wgs1.usc
Unit Set:	NewUser
Date/Time:	Friday Jun 28 2013, 18:13:35

Material Stream: 15 (continued)

Fluid Package:	Basis-1
Property Package:	Peng-Robinson

COMPOSITION

Liquid Phase (continued)   Phase Fraction   0.0000

COMPONENTS	MOLAR FLOW (kgmole/h)	MOLE FRACTION	MASS FLOW (kg/h)	MASS FRACTION	LIQUID VOLUME FLOW (m3/h)	LIQUID VOLUME FRACTION
H2O	0.0000	0.7766	0.0000	0.7302	0.0000	0.6049
H2S	0.0000	0.0000	0.0000	0.0000	0.0000	0.0000
Air	0.0000	0.0000	0.0000	0.0000	0.0000	0.0000
Oxygen	0.0000	0.0000	0.0000	0.0000	0.0000	0.0000
Nitrogen	0.0000	0.0000	0.0000	0.0000	0.0000	0.0000
Total	0.0000	1.0000	0.0000	1.0000	0.0000	1.0000

Aqueous Phase   Phase Fraction   0.0000

COMPONENTS	MOLAR FLOW (kgmole/h)	MOLE FRACTION	MASS FLOW (kg/h)	MASS FRACTION	LIQUID VOLUME FLOW (m3/h)	LIQUID VOLUME FRACTION
Methane	0.0000	0.0001	0.0000	0.0001	0.0000	0.0003
Ethane	0.0000	0.0000	0.0000	0.0000	0.0000	0.0000
Propane	0.0000	0.0000	0.0000	0.0000	0.0000	0.0000
i-Butane	0.0000	0.0000	0.0000	0.0000	0.0000	0.0000
i-Pentane	0.0000	0.0000	0.0000	0.0000	0.0000	0.0000
Hydrogen	0.0000	0.1092	0.0000	0.0115	0.0000	0.1360
CO2	0.0000	0.1096	0.0000	0.2518	0.0000	0.2523
CO	0.0000	0.0043	0.0000	0.0063	0.0000	0.0066
H2O	0.0000	0.7766	0.0000	0.7302	0.0000	0.6049
H2S	0.0000	0.0000	0.0000	0.0000	0.0000	0.0000
Air	0.0000	0.0000	0.0000	0.0000	0.0000	0.0000
Oxygen	0.0000	0.0000	0.0000	0.0000	0.0000	0.0000
Nitrogen	0.0000	0.0000	0.0000	0.0000	0.0000	0.0000
Total	0.0000	1.0000	0.0000	1.0000	0.0000	1.0000

Material Stream: 24

Fluid Package:	Basis-1
Property Package:	Peng-Robinson

CONDITIONS

		Overall	Vapour Phase			
Vapour / Phase Fraction		1.0000 *	1.0000			
Temperature:	(C)	50.00 *	50.00			
Pressure:	(bar)	1.500 *	1.500			
Molar Flow	(gmole/min)	0.5585	0.5585			
Mass Flow	(g/min)	12.93	12.93			
Std Ideal Liq Vol Flow	(mL/min)	22.90	22.90			
Molar Enthalpy	(kJ/kgmole)	-1.947e+005	-1.947e+005			
Molar Entropy	(kJ/kgmole-C)	153.9	153.9			
Heat Flow	(kJ/h)	-6524	-6524			
Liq Vol Flow @Std Cond	(mL/min)	----	---			

COMPOSITION

Overall Phase   Vapour Fraction   1.0000 *

COMPONENTS	MOLAR FLOW (kgmole/h)	MOLE FRACTION	MASS FLOW (kg/h)	MASS FRACTION	LIQUID VOLUME FLOW (m3/h)	LIQUID VOLUME FRACTION
Methane	0.0000	0.0006	0.0003	0.0004	0.0000	0.0008
Ethane	0.0000	0.0000	0.0000	0.0000	0.0000	0.0000
Propane	0.0000	0.0000	0.0000	0.0000	0.0000	0.0000
i-Butane	0.0000	0.0000	0.0000	0.0000	0.0000	0.0000
i-Pentane	0.0000	0.0000	0.0000	0.0000	0.0000	0.0000
Hydrogen	0.0164	0.4890	0.0330	0.0426	0.0005	0.3442
CO2	0.0165	0.4909	0.7240	0.9335	0.0009	0.6384
CO	0.0007	0.0194	0.0182	0.0235	0.0000	0.0166

K

Honeywell	Company Name Not Available Calgary, Alberta CANADA	Case Name: C:\Users\Christian\Desktop\wgs1.usc
		Unit Set: NewUser
		Date/Time: Friday Jun 28 2013, 18:13:35

Material Stream: 24 (continued)

Fluid Package: Basis-1

Property Package: Peng-Robinson

COMPOSITION

Overall Phase (continued)

Vapour Fraction   1.0000 *

COMPONENTS	MOLAR FLOW (kgmole/h)	MOLE FRACTION	MASS FLOW (kg/h)	MASS FRACTION	LIQUID VOLUME FLOW (m3/h)	LIQUID VOLUME FRACTION
H2O	0.0000	0.0000	0.0000	0.0000	0.0000	0.0000
H2S	0.0000	0.0000	0.0000	0.0000	0.0000	0.0000
Air	0.0000	0.0000	0.0000	0.0000	0.0000	0.0000
Oxygen	0.0000	0.0000	0.0000	0.0000	0.0000	0.0000
Nitrogen	0.0000	0.0000	0.0000	0.0000	0.0000	0.0000
Total	0.0335	1.0000	0.7756	1.0000	0.0014	1.0000

Vapour Phase

Phase Fraction   1.000

COMPONENTS	MOLAR FLOW (kgmole/h)	MOLE FRACTION	MASS FLOW (kg/h)	MASS FRACTION	LIQUID VOLUME FLOW (m3/h)	LIQUID VOLUME FRACTION
Methane	0.0000	0.0006	0.0003	0.0004	0.0000	0.0008
Ethane	0.0000	0.0000	0.0000	0.0000	0.0000	0.0000
Propane	0.0000	0.0000	0.0000	0.0000	0.0000	0.0000
i-Butane	0.0000	0.0000	0.0000	0.0000	0.0000	0.0000
i-Pentane	0.0000	0.0000	0.0000	0.0000	0.0000	0.0000
Hydrogen	0.0164	0.4890	0.0330	0.0426	0.0005	0.3442
CO2	0.0165	0.4909	0.7240	0.9335	0.0009	0.6384
CO	0.0007	0.0194	0.0182	0.0235	0.0000	0.0166
H2O	0.0000	0.0000	0.0000	0.0000	0.0000	0.0000
H2S	0.0000	0.0000	0.0000	0.0000	0.0000	0.0000
Air	0.0000	0.0000	0.0000	0.0000	0.0000	0.0000
Oxygen	0.0000	0.0000	0.0000	0.0000	0.0000	0.0000
Nitrogen	0.0000	0.0000	0.0000	0.0000	0.0000	0.0000
Total	0.0335	1.0000	0.7756	1.0000	0.0014	1.0000

Honeywell International Inc.   UniSim Design (R400 Build 16067)   Page 4 of 4

Licensed to: Company Name Not Available   Printed by: Christian   * Specified by user.

L

Activation Energy Inlet data

		m=	4.8 mg																	
	T	P	K	H2			CO			CO2			H2O			He			Fin	GHSV
	°C	Pa		mL/min	%	kPa	mL/min	%	kPa	mL/min	%	kPa	mL/min	%	kPa	mL/min	%	kPa	mL/min	cm3/gcat*
1	475	1.50E+05	7.39	90	17.3	26	50	9.6	14.4	80	15.4	23.1	200	38.5	57.7	100	19.2	28.8	520	6500000
2	450	1.50E+05	7.39	90	17.3	26	50	9.6	14.4	80	15.4	23.1	200	38.5	57.7	100	19.2	28.8	520	6500000
3	425	1.50E+05	7.39	90	17.3	26	50	9.6	14.4	80	15.4	23.1	200	38.5	57.7	100	19.2	28.8	520	6500000
4	400	1.50E+05	7.39	90	17.3	26	50	9.6	14.4	80	15.4	23.1	200	38.5	57.7	100	19.2	28.8	520	6500000

Table F1a.- Inlet conditions for Activation energy experimental calculations. 3.0Pd/20Ni-20Co HT sample

		m=	4.8																		
	T	P	K	H2	CH4	CO	CO2	P CO2	P CO	P H2	PCH4	P H2O	Xmeth	Xwgs	β	Dipersion	r	rf	TOF	ln(TOF)	1000/RT
	°C	Pa		%	%	%	%						%	%			mol/gcat*s		seg-1		
1	475	1.50E+05	7.39	26.063	0.193	10.594	25.74	0.22238	0.08651	0.24127	0.00167	0.44818	1.39597	26.1778	0.18721	0.065	0.01111	0.01367	13.0958	2.57229	0.1608
2	450	1.50E+05	7.39	25.5785	0.1365	10.982	24.836	0.21891	0.09016	0.23916	0.0012	0.45057	1.0082	23.4399	0.17436	0.065	0.01019	0.01234	11.8258	2.47028	0.16636
3	425	1.50E+05	7.39	25.4706	0.0728	12.6754	23.886	0.20886	0.10043	0.23079	0.00064	0.4593	0.53402	15.2157	0.14138	0.065	0.0068	0.00792	7.58804	2.02657	0.17232
4	400	1.50E+05	7.39	25.667	0.06	11.503	23.24	0.20496	0.10437	0.2272	0.00053	0.46295	0.44401	11.9806	0.13039	0.065	0.00556	0.0064	6.12997	1.81319	0.17872

Table F1b.- Inlet conditions for Activation energy experimental calculations. 4.5Pd/20Ni-20Co HT sample

Activation Energy outlet data

	m=	4.8 mg																		
	T	P	K	H2			CO			CO2			H2O			He			Fin	GHSV
	°C	Pa		mL/min	%	kPa	mL/min	%	kPa	mL/min	%	kPa	mL/min	%	kPa	mL/min	%	kPa	mL/min	cm3/gcat*h
1	475	1.50E+05	7.39	90	17.3	26	50	9.6	14.4	80	15.4	23.1	200	38.5	57.7	100	19.2	28.8	520	6500000
2	450	1.50E+05	7.39	90	17.3	26	50	9.6	14.4	80	15.4	23.1	200	38.5	57.7	100	19.2	28.8	520	6500000
3	425	1.50E+05	7.39	90	17.3	26	50	9.6	14.4	80	15.4	23.1	200	38.5	57.7	100	19.2	28.8	520	6500000
4	400	1.50E+05	7.39	90	17.3	26	50	9.6	14.4	80	15.4	23.1	200	38.5	57.7	100	19.2	28.8	520	6500000

Table F1a*.- Outlet measurements from GC and kinetic calculations for activation energy, 3.0Pd/20Ni-20Co HT sample

	m=	4.8																				
	T	P	K	H2	CH4	CO	CO2	P CO2	P CO	P H2	PCH4	P H2O	Xwgs	β	Dipersion	n	r	rf	TOF	ln(TOF)	1000/RT
	°C	Pa		%	%	%	%						%				mol/gcat*s	seg-1			
1	475	1.50E+05	7.39	25.9132	0.22767	9.91461	26.1693	0.22872	0.08004	0.24666	0.00199	0.44259	31.3669	0.21545	0.039	1.93E-06	0.01331	0.01696	27.0878	3.29908	0.1608
2	450	1.50E+05	7.39	26.1648	0.136	10.7563	25.615	0.21999	0.08909	0.24035	0.00117	0.4494	24.3601	0.17866	0.039	2.00E-06	0.01056	0.01286	20.535	3.02213	0.16636
3	425	1.50E+05	7.39	25.9329	0.18114	11.4964	25.1943	0.2156	0.09333	0.23484	0.00155	0.45468	20.5471	0.16142	0.039	2.07E-06	0.00943	0.01125	17.9605	2.88817	0.17232
4	400	1.50E+05	7.39	25.1342	0.07039	12.2281	24.5961	0.20961	0.09969	0.23165	0.0006	0.45846	15.8597	0.14373	0.039	2.15E-06	0.00733	0.00856	13.6647	2.61482	0.17872

Table F1b*.- Outlet measurements from GC and kinetic calculations for activation energy, 4.5Pd/20Ni-20Co HT sample

H2 Order Inlet data

		m=		4.8 mg																
	T	P	K	H2			CO			CO2			H2O			He			Fin	GHSV
	°C	Pa		mL/min	%	kPa	mL/min	%	kPa	mL/min	%	kPa	mL/min	%	kPa	mL/min	%	kPa	mL/min	cm3/gcat*h
1	450	1.50E+05	7.39	110	21.2	31.7	50	9.6	14.4	80	15.4	23.1	200	38.5	57.7	80	15.4	23.1	520	6500000
2	450	1.50E+05	7.39	90	17.3	26	50	9.6	14.4	80	15.4	23.1	200	38.5	57.7	100	19.2	28.8	520	6500000
3	450	1.50E+05	7.39	80	15.4	23.1	50	9.6	14.4	80	15.4	23.1	200	38.5	57.7	110	21.2	31.7	520	6500000
4	450	1.50E+05	7.39	50	9.6	14.4	50	9.6	14.4	80	15.4	23.1	200	38.5	57.7	140	26.9	40.4	520	6500000
5	450	1.50E+05	7.39	35	6.7	10.1	50	9.6	14.4	80	15.4	23.1	200	38.5	57.7	155	29.8	44.7	520	6500000
6	450	1.50E+05	7.39	20	3.8	5.8	50	9.6	14.4	80	15.4	23.1	200	38.5	57.7	170	32.7	49	520	6500000

Table F2a.- Inlet conditions for H2 order experimental calculations. 3.0Pd/20Ni-20Co HT sample

		m=		4.8 mg																
	T	P	K	H2			CO			CO2			H2O			He			Fin	GHSV
	°C	Pa		mL/min	%	kPa	mL/min	%	kPa	mL/min	%	kPa	mL/min	%	kPa	mL/min	%	kPa	mL/min	cm3/gcat*h
1	450	1.50E+05	7.39	110	21.2	31.7	50	9.6	14.4	80	15.4	23.1	200	38.5	57.7	80	15.4	23.1	520	6500000
2	450	1.50E+05	7.39	90	17.3	26	50	9.6	14.4	80	15.4	23.1	200	38.5	57.7	100	19.2	28.8	520	6500000
3	450	1.50E+05	7.39	80	15.4	23.1	50	9.6	14.4	80	15.4	23.1	200	38.5	57.7	110	21.2	31.7	520	6500000
4	450	1.50E+05	7.39	50	9.6	14.4	50	9.6	14.4	80	15.4	23.1	200	38.5	57.7	140	26.9	40.4	520	6500000
5	450	1.50E+05	7.39	35	6.7	10.1	50	9.6	14.4	80	15.4	23.1	200	38.5	57.7	155	29.8	44.7	520	6500000

Table F1b.- Inlet conditions for H2 order experimental calculations. 4.5Pd/20Ni-20Co HT sample

H2 Order outlet data

| | m= | 4.8 | | | | | | | | | | | | | | | | | | | | | | |

	T	P	K	H2	CH4	CO	CO2	P CO2	P CO	P H2	PCH4	P H2O	Xmeth	Xwgs	β	Dipersion	n	r	rf	TOF	ln(TOF)	ln(rf)	PCO	Ln(PH2)
	°C	Pa		%	%	%	%						%	%			mol/seg	mol/gcat*s		seg-1			Mol frac	
1	450	1.50E+05	7.39	30.328	0.31	12.2265	23.3238	0.20267	0.09168	0.26314	0.00269	0.43981	2.35783	17.3979	0.17894	0.065	2.00E-06	0.0082336	0.01003	9.66158	2.26816	-4.60237	0.1133	3.45729
2	450	1.50E+05	7.39	25.5785	0.1365	10.982	24.836	0.21891	0.09016	0.23916	0.0012	0.45057	1.0082	23.4399	0.17436	0.065	2.00E-06	0.0101892	0.01234	11.8258	2.47028	-4.39483	0.1133	3.25662
3	450	1.50E+05	7.39	23.4845	0.1335	9.001	25.41	0.27645	0.09461	0.10016	0.00145	0.52733	1.01374	32.952	0.07391	0.065	2.00E-06	0.0141559	0.01529	14.7271	2.68969	-4.18084	-1.97188	3.13883
4	450	1.50E+05	7.39	15.9673	0.07243	10.061	25.271	0.26987	0.10136	0.09586	0.00077	0.53214	0.54062	28.6168	0.06151	0.065	2.00E-06	0.0121519	0.01295	12.4753	2.52375	-4.34678	-0.97188	2.66883
5	450	1.50E+05	7.39	12.2923	0.041	9.57733	25.8767	0.26988	0.10144	0.09702	0.00043	0.53124	0.29907	28.7521	0.0512	0.065	2.00E-06	0.0121076	0.01276	12.2947	2.50917	-4.36136	0.02812	2.31215
6	450	1.50E+05	7.39	9.37567	0.01033	10.3233	25.176	0.25655	0.11485	0.08477	0.00011	0.54373	0.07369	19.5464	0.04711	0.065	2.00E-06	0.008177	0.00858	8.26777	2.11236	-4.75817	2.02812	1.75254

Table F2a*.- Outlet measurements from GC and kinetic calculations for H2 Order, 3.0Pd/20Ni-20Co HT sample

| | m= | 4.8 | | | | | | | | | | | | | | | | | | | | | | |

	T	P	K	H2	CH4	CO	CO2	P CO2	P CO	P H2	PCH4	P H2O	Xmeth	Xwgs	β	Dipersion	n	r	rf	TOF	ln(TOF)	ln(rf)	PCO	Ln(PH2)
	°C	Pa		%	%	%	%						%	%			mol/seg	mol/gcat*s		seg-1			Mol frac	
1	450	1.50E+05	7.39	29.0905	0.0915	12.539	24.5728	0.20503	0.09011	0.27102	0.00076	0.43307	0.67082	20.1508	0.19264	0.039	2.00E-06	0.0086778	0.01075	17.166	2.84293	-4.533	0.1133	3.45729
2	450	1.50E+05	7.39	25.7423	0.136	10.7563	25.615	0.21999	0.08909	0.24035	0.00117	0.4494	0.97884	24.3601	0.17866	0.039	2.00E-06	0.0105554	0.01285	20.5251	3.02165	-4.35429	0.1133	3.25662
3	450	1.50E+05	7.39	23.1445	0.1345	9.038	25.31	0.27586	0.09519	0.09953	0.00147	0.52795	0.67082	32.5382	0.07391	0.039	2.00E-06	0.0138338	0.01494	23.8572	3.17209	-4.20385	-1.97188	3.13883
4	450	1.50E+05	7.39	15.0973	0.06333	10.271	25.139	0.26757	0.1037	0.09411	0.00061	0.53401	0.47179	27.2671	0.06151	0.039	2.00E-06	0.0115552	0.01231	19.6643	2.9788	-4.39714	-0.97188	2.66883
5	450	1.50E+05	7.39	11.2923	0.033	10.5773	25.0837	0.2601	0.11124	0.08753	0.00034	0.54079	0.23937	21.9476	0.0512	0.039	2.00E-06	0.0092424	0.00974	15.5576	2.74455	-4.63139	0.02812	2.31215

Table F2b*.- Outlet measurements from GC and kinetic calculations for H2 Order, 4.5Pd/20Ni-20Co HT sample

CO order inlet data

| m= | 4.8 mg |

	T	P	K	H2			CO			CO2			H2O			He			Fin
	°C	Pa		mL/min	%	kPa	mL/min	%	kPa	mL/min	%	kPa	mL/min	%	kPa	mL/min	%	kPa	mL/min
1	450	1.50E+05	7.39	90	17.3	26.0	80	15.4	23.1	80	15.4	23.1	200	38.5	57.7	70	13.5	20.2	520
2	450	1.50E+05	7.39	90	17.3	26.0	50	9.6	14.4	80	15.4	23.1	200	38.5	57.7	100	19.2	28.8	520
3	450	1.50E+05	7.39	90	17.3	26.0	20	3.8	5.8	80	15.4	23.1	200	38.5	57.7	130	25.0	37.5	520

Table F3a.- Inlet conditions for CO order experimental calculations. 3.0Pd/20Ni-20Co HT sample

| m= | 4.8 mg |

	T	P	K	H2			CO			CO2			H2O			He			Fin
	°C	Pa		mL/min	%	kPa	mL/min	%	kPa	mL/min	%	kPa	mL/min	%	kPa	mL/min	%	kPa	mL/min
1	450	1.50E+05	7.39	90	17.3	26	80	15.4	23.1	80	15.4	23.1	200	38.5	57.7	70	13.5	20.2	520
2	450	1.50E+05	7.39	90	17.3	26	50	9.6	14.4	80	15.4	23.1	200	38.5	57.7	100	19.2	28.8	520
3	450	1.50E+05	7.39	90	17.3	26	20	3.8	5.8	80	15.4	23.1	200	38.5	57.7	130	25	37.5	520

Table F3b.- Inlet conditions for CO order experimental calculations. 4.5Pd/20Ni-20Co HT sample

CO Order Outled data

	m=	4.8																					
	T	P	K	H2	CH4	CO	CO2	P CO2	P CO	P H2	PCH4	P H2O	Xmeth	Xwgs	β	Dipersion	r	rf	TOF	ln(TOF)	ln(rf)	PCO	ln(PCO)
	°C	Pa		%	%	%	%						%	%			mol/gcat*s		seg-1			Mol frac	
1	450	1.50E+05	7.39	26.4076	0.0524	19.5102	25.9494	0.20414	0.15129	0.22515	0.00041	0.41901	0.23169	14.7354	0.09809	0.065	0.01597	0.01771	16.968	2.83133	-4.03388	0.1133	3.13883
2	450	1.50E+05	7.39	25.5785	0.1365	10.982	24.836	0.21891	0.09016	0.23916	0.0012	0.45057	1.0082	23.4399	0.17436	0.065	0.01019	0.01234	11.8269	2.47038	-4.39483	0.07055	2.66883
3	450	1.50E+05	7.39	24.7584	0.02586	4.84871	25.1004	0.22092	0.03538	0.24589	0.00023	0.49759	0.44357	30.5915	0.41741	0.065	0.00207	0.00355	3.40427	1.22503	-5.64018	0.02812	1.75254

Table F2a*.- Outlet measurements from GC and kinetic calculations for CO Order, 3.0Pd/20Ni-20Co HT sample

	m=	4.8																					
	T	P	K	H2	CH4	CO	CO2	P CO2	P CO	P H2	PCH4	P H2O	Xmeth	Xwgs	β	Dipersion	r	rf	TOF	ln(TOF)	ln(rf)	PCO	ln(PCO)
	°C	Pa		%	%	%	%						%	%			mol/gcat*s		seg-1			Mol frac	
1	450	1.50E+05	7.39	26.1555	0.08975	16.7763	25.594	0.21348	0.14186	0.23349	0.00075	0.41042	0.42046	19.903	0.11582	0.039	0.02168	0.02452	39.1673	3.66784	-3.7081	0.1133	3.13883
2	450	1.50E+05	7.39	26.1648	0.136	10.7563	25.615	0.21999	0.08909	0.24035	0.00117	0.4494	0.97884	24.3601	0.17866	0.039	0.01056	0.01286	20.535	3.02213	-4.35381	0.07055	2.66883
3	450	1.50E+05	7.39	25.4146	0.0612	4.2092	24.322	0.22524	0.0309	0.24921	0.00057	0.49409	1.10392	38.7189	0.49747	0.039	0.00266	0.00528	8.43946	2.13292	-5.24302	0.02812	1.75254

Table F3b*.- Outlet measurements from GC and kinetic calculations for CO Order, 4.5Pd/20Ni-20Co HT sample

Appendix G

<table>
<tr><td>Flow</td><td></td><td></td><td>SEWGS Time on stream</td></tr>
<tr><td>0.5585 gmol/min</td><td></td><td></td><td>54.5 min</td></tr>
</table>

	Dry molar fraction					Molar Flow (mol/min)				Average steady flow		
	Time on stream	H2	CH4	CO	CO2	H2	CO2	CH4		0.54	0.00	0.01
SEWGS	0.00	89.03279	0.47	10.49	0.00	0.50	0.00	0.00				
	3.43	99.29	0.70	0.00	0.00	0.55	0.00	0.00		Average SEWGS flow		
	6.87	98.90	0.71	0.39	0.00	0.55	0.00	0.00		0.26	0.29	0.01
	10.30	99.22	0.69	0.09	0.00	0.55	0.00	0.00				
	13.73	99.18	0.78	0.03	0.00	0.55	0.00	0.00		Δn_w during time on stream		
	17.16	99.02	0.94	0.03	0.01	0.55	0.00	0.01		15.6219	-15.6013	-0.08387
	20.59	98.82	1.14	0.03	0.01	0.55	0.00	0.01				
	24.02	98.61	1.36	0.03	0.01	0.55	0.00	0.01		m produced or inhibed (gms)		
	27.45	98.57	1.42	0.00	0.01	0.55	0.00	0.01		31.2439	-686.459	-1.3419
	30.88	98.51	1.46	0.02	0.02	0.55	0.00	0.01				
	34.31	98.09	1.87	0.03	0.01	0.55	0.00	0.01				
	37.74	98.34	1.63	0.01	0.02	0.55	0.00	0.01				
	41.17	97.95	2.03	0.00	0.02	0.55	0.00	0.01				
	44.60	97.77	2.18	0.02	0.03	0.55	0.00	0.01				
	48.03	97.84	2.10	0.02	0.04	0.55	0.00	0.01				
	51.46	95.60	2.63	0.07	1.70	0.53	0.01	0.01				
	54.89	89.81	2.07	0.20	7.93	0.50	0.04	0.01				
Transition	58.32	77.87	2.27	0.36	19.50	0.43	0.11	0.01				
	61.75	67.26	1.88	0.59	30.26	0.38	0.17	0.01				
	65.18	55.36	1.69	0.80	42.14	0.31	0.24	0.01				
	68.61	47.94	1.86	0.88	50.19	0.27	0.28	0.01				
	72.04	48.16	1.46	0.98	49.40	0.27	0.28	0.01				
	75.47	46.72	1.91	0.88	51.38	0.26	0.29	0.01				
	78.90	47.29	1.40	0.85	51.31	0.26	0.29	0.01				
	82.33	46.23	1.76	0.88	51.13	0.26	0.29	0.01				
HTS	85.76	46.55	1.59	0.97	50.88	0.26	0.28	0.01				
	89.19	47.25	1.61	0.97	51.14	0.26	0.29	0.01				
	92.62	41.75	1.90	0.96	55.39	0.23	0.31	0.01				
	96.05	42.65	1.60	0.91	55.75	0.24	0.31	0.01				
	99.48	45.47	1.90	0.86	51.77	0.25	0.29	0.01				

Table G1.- SEWGS balance according to the average HTS molar flow. Reaction conditions 450°C, 1.5 atm, volumetric water flow of 40 ml/min and 10 ml/min of CO, catalyst preparation of .4 mg of 3.0Pd/20Ni-20Co HT and 4 gms of dolomite.

FLOW: 0.5585 gmol/min
SEWGS Time on stream: 51.5 min

Section	Dry molar fraction					Molar Flow (mol/min)		
	Time on stream	H2	CH4	CO	CO2	H2	CO2	CH4
SEWGS	00:00:00	96.94	0.25	2.82	0.00	0.54	0.00	0.00
SEWGS	3.43	99.34	0.27	0.39	0.00	0.55	0.00	0.00
SEWGS	6.87	99.61	0.31	0.08	0.00	0.56	0.00	0.00
SEWGS	10.3	99.53	0.43	0.04	0.00	0.56	0.00	0.00
SEWGS	13.73	99.34	0.63	0.02	0.00	0.55	0.00	0.00
SEWGS	17.16	98.99	0.98	0.02	0.01	0.55	0.00	0.01
SEWGS	20.59	98.62	1.35	0.03	0.00	0.55	0.00	0.01
SEWGS	24.02	98.40	1.57	0.02	0.00	0.55	0.00	0.01
SEWGS	27.45	98.11	1.87	0.01	0.00	0.55	0.00	0.01
SEWGS	30.88	97.87	2.11	0.02	0.00	0.55	0.00	0.01
SEWGS	34.31	97.61	2.36	0.02	0.01	0.55	0.00	0.01
SEWGS	37.74	97.38	2.60	0.01	0.01	0.54	0.00	0.01
SEWGS	41.17	97.12	2.86	0.00	0.01	0.54	0.00	0.02
SEWGS	44.6	96.82	3.14	0.03	0.02	0.54	0.00	0.02
SEWGS	48.03	96.21	3.33	0.04	0.42	0.54	0.00	0.02
SEWGS	51.46	91.94	3.52	0.12	4.41	0.51	0.02	0.02
Transition	54.89	80.34	3.31	0.30	16.05	0.45	0.09	0.02
Transition	58.32	65.31	2.80	0.49	31.39	0.36	0.18	0.02
Transition	61.75	51.62	2.97	0.67	44.73	0.29	0.25	0.02
Transition	65.18	44.70	2.85	0.77	51.69	0.25	0.29	0.02
Transition	68.61	42.44	2.80	0.78	53.98	0.24	0.30	0.02
HTS	72.04	41.81	2.85	0.79	54.55	0.23	0.30	0.02
HTS	75.47	41.67	2.74	0.79	54.80	0.23	0.31	0.02
HTS	78.9	41.65	2.78	0.80	54.77	0.23	0.31	0.02
HTS	82.33	41.58	2.73	0.79	54.90	0.23	0.31	0.02
HTS	85.76	41.59	2.76	0.79	54.85	0.23	0.31	0.02
HTS	89.19	41.44	2.70	0.80	55.06	0.23	0.31	0.02
HTS	92.62	41.46	2.77	0.80	54.98	0.23	0.31	0.02
HTS	96.05	41.52	2.71	0.79	54.98	0.23	0.31	0.02
HTS	99.48	41.77	2.73	0.79	55.49	0.23	0.31	0.02

Average steady flow: 0.54588 | 0.00172 | 0.00963
Average SEWGS flow: 0.23227 | 0.30662 | 0.01536
Δn_W during time on stream: 16.1506 | -15.7026 | -0.29552
m produced or inhibed (gms): 32.3012 | -690.913 | -4.72828

Table G1.- SEWGS balance according to the average HTS molar flow. Reaction conditions 450°C, 1.5 atm, volumetric water flow of 40 ml/min and 10 ml/min of CO, catalyst preparation of .4 mg of 4.5Pd/20Ni-20Co HT and 4 gms of dolomite.